Permafrost distribution in steep slopes in Norway: measurements, statistical modelling and geomorphological implications

Florence Magnin[1], Bernd Etzelmüller[1], Sebastian Westermann[1], Ketil Isaksen[2], Paula Hilger[1,3], Reginald L. Hermanns[3,4]

[1] Department of Geosciences, University of Oslo, Oslo, 0316, Norway
[2] The Norwegian Meteorological Institute, Oslo, 0313, Norway
[3] Geohazards and Earth observation, Geological Survey of Norway, Trondheim, 7040, Norway
[4] Institute for Geoscience and Petroleum, Norwegian University of Science and Technology, Trondheim, Norway

Correspondence to: Florence Magnin (florence.magnin@geo.uio.no)

Abstract. Permafrost in steep slopes has been increasingly studied since the early 2000s in conjunction with a growing number of rock-slope failures, which likely resulted from permafrost degradation. In Norway, rock-slope destabilization is a widespread phenomenon and a major source of risk for the population and infrastructure. However, the lack of precise understanding of the permafrost distribution in steep slopes hinders the assessment of its role in these destabilizations. This study proposes the first nation-wide permafrost probability map for the steep slopes of Norway (CryoWall map). It is based on a multiple linear regression model fitted with multi-annual rock surface temperature (RST) measurements, collected at 25 rock-wall sites, spread across a latitudinal transect (59-69°N) over mainland Norway. The CryoWall map suggests that discontinuous permafrost widely occurs above 1300-1400 and 1600-1700 m a.s.l. in the north and south slopes of southern Norway (59°N), respectively. This lower altitudinal limit decreases in northern Norway (70°N) by about 500±50 m, with more pronounced decrease for south faces, in reason of the insolation patterns largely driven by midnight sun in summer and polar night in winter. Similarly, the mean annual RST differences between north and south faces of similar elevation range around 1.5°C in northern Norway and 3.5°C in southern Norway. The CryoWall map is evaluated against direct ice observations in steep slopes and discussed in the context of former permafrost studies in various types of terrains in Norway. We show that permafrost can occur at much lower elevations in steep rock slopes than in other terrains, especially in north faces. We demonstrate that the CryoWall map is a valuable basis for further investigations related to permafrost in steep slopes in both practical concerns and fundamental science.

1 Introduction

Permafrost affecting steep bedrock slopes has been increasingly studied since the early 2000s in conjunction with both the high frequency of rock-fall activity during hot summers (*e.g.* Gruber et al., 2004a; Fischer et al., 2006 ; Allen et al., 2009; Ravanel et al., 2017), and the occurrence of high-magnitude rock-ice avalanches (*e.g.* Haeberli et al., 2004; Sosio et al., 2008; Huggel et al., 2012; Deline et al., 2015).

Permafrost processes affect rock-wall stability as much on short as on long time scales (days to millennia), by modifying the bedrock and ice-mechanical properties (Krautblatter et al., 2013). Permafrost aggradation provokes ice segregation processes, which prepare high-magnitude slope failure by favouring fracture propagation at depth (Matsuoka and Murton, 2008). Permafrost degradation can critically modify the shear strength of ice-filled fractures, with the most critical conditions being between -2 and 0°C (Davies et al., 2001). Water circulating in ice-free or partly ice-filled fractures could also accelerate the melting of ice in joints (Hasler et al., 2011a), while hydrostatic pressures caused by hydraulic permeability of ice-sealed fractures also adds to slope destabilization (Fischer et al., 2010). Rock-slope failures jeopardize infrastructures, activities and individuals in the either by direct hit or by potential secondary effects, such as displacement waves and catastrophic flooding through debris flows (e.g. Huggel et al., 2005; Romstad et al., 2009, Hermanns et al., 2013).

Finally, rock fall and rock avalanches are essential agents of periglacial and paraglacial mass wasting processes (Ballantyne, 2002), and mass wasting and sediment transport sources in general (Korup, 2009). The role of the thermal regime as a significant driver for landscape forming processes has been emphasized recently (Berthling and Etzelmuller, 2011), and developed in modelling approaches to understand landscaping processes (e.g. Hales and Roering, 2007; Egholm et al., 2015). It is evident that the understanding of thermal regime within mountain slopes, and its development during past and the future, has significant relevance for geomorphology.

In Norway, the glacially shaped deep valleys and fjords are prone to mass-wasting processes. Rock-slope failures from the oversteepened slopes and potential secondary effects, such as displacement waves, represent one of the most deadly natural hazards in the country (Furseth, 2006; Hermanns et al., 2012). Over the last 500 years, approximately 800 events and 500 fatalities have been recorded throughout the country, among which three displacement waves, triggered by major rock-slope failures, caused the loss of 175 lives during the 20th century (Furseth, 2006; Hermanns et al., 2013; 2014). At present, more than 253 unstable rock slopes have been mapped systematically, and are partly monitored periodically by the Norwegian geological survey (Oppikofer et al., 2015). At one of seven rock-slope instabilities, that are continuously monitored because of the potentially severe consequences in case of failure, direct observations allowed for a detailed assessment about the role of permafrost in local rock-wall dynamics (Blikra and Christiansen, 2014). Many of these unstable slopes are most likely located at or above the lower boundary of altitudinal permafrost (Hilger et al., 2018). However, the lack of knowledge about its precise distribution in steep slopes precludes a systematic assessment of its role in the conditioning of rock slope failures.

Permafrost monitoring networks have been deployed in gentle mountain slopes and mires of northern and southern Norway in the frame of national and international research programs (Ødegård et al., 1992; Harris et al., 2001; Christiansen et al., 2010; Isaksen et al., 2011; Farbrot et al., 2011). Numerical models have been used to

assess the permafrost distribution at the national and Scandinavian scales (Westermann et al., 2013; Gisnås et al., 2013; 2016; 2017). The study of permafrost in steep slopes in Norway has recently started with direct measurements of rock surface temperature (RST) in the high-elevated alpine areas of Jotunheimen and Hurrungane (Hipp et al., 2014). Myhra et al. (2017) have simulated the permafrost evolution since the end of the Little Ice Age (1880) to present, for steep mountain sites spread over a latitudinal transect over Norway. At the national scale, a first-order estimation of the permafrost distribution in steep slopes has been proposed by Steiger et al., (2016), based on a straight forward empirical relationship between air and rock-wall surface temperatures. Finally, Frauenfelder et al. (2018) studied ground thermal and geomechanical conditions in a permafrost-affected rockslide site in Troms (northern Norway). It is likely that changing rock and ice-temperatures, due to general warming and in response to the extreme warm previous year, have played an important role in this detachment.

Knowing the current distribution of permafrost is a prerequisite to assess its past, present and future variability, as well as to provide key-knowledge and tools to landuse-planners and geomorphologists. Thus, the lack of precise knowledge regarding the nation-wide distribution of steep slope permafrost is a major gap for both fundamental research and practical concerns. Therefore, we have monitored the RST at 25 measurement points, covering various aspects and elevations across a latitudinal transect of Norway to (i) characterize the thermal regime in steep slopes, (ii) calibrate a statistical model of RST and (iii) map permafrost probability for steep slopes at the national scale. In this paper, we present (i) the measurement settings and strategy, (ii) the approaches for statistical modelling and permafrost probability mapping, and (iii) the permafrost distribution in steep slopes at the national scale and for local areas of interest.

2 Study area

The Norwegian mainland has a land area of c. 350000 km^2, and is dominated by the mountain chain of the Scandes, stretching between 57 – 71 °N through Norway and Sweden over a distance of more than 2000 km. Scandinavia forms a tilted margin, with highest elevations found towards the western coast, decreasing towards the east and the Bothnian Sea. The area has undergone multiple glaciations during the Pleistocene, with the largest glaciations covering northern Europe completely several times during the last c. 1 Mio. yrs (e.g. Kleman et al 2008). Most of the land area in Norway is dominated by gentle relief landscape (Etzelmüller et al., 2007), probably preserved under cold-based ice conditions during the major glaciations (e.g. Kleman et al., 1999). Steep slopes and rock walls are mainly associated to four types of settings (e.g. Steiger et al., 2016): (i) steep valley sides associated to large U-shaped valleys which drained the ice sheets during the glaciations, (ii) rock walls formed by local glaciations, mostly located along the western coast of the country and within the highest mountain regions of central southern Norway, (iii) rock walls associated to overthrusted nappes, such as in Hallingskarvet, and (iv) rock walls associated to steep river incisions, such as Alta canyon (*Čávžu* in Sami) in Finnmark. High-relief areas of Norway have experienced a high rock-slope failure activity throughout the late Pleistocene and Holocene, with a peak shortly after deglaciation (Böhme et al. 2015, Hermanns et al. 2017). The result is a high density of rock-slope failure deposits and colluvial slopes (e.g. Hilger et al 2018), both in western and northern Norway. The occurrence of actively deforming rock-slope instabilities demonstrates the ongoing paraglacial landscape response towards natural stability equilibrium.

In general, the lower limit of mountain permafrost in Scandinavia decreases from the western coast towards eastern Norway and north-western Sweden, while the glaciation limit increases from west to east (e.g. King, 1983, 1986; Etzelmüller et al., 2003a). These gradients follow the climatic setting, with the maritime climate along the western coast (moist and high snow cover) gradually changing towards a more continental climate in the eastern parts of Norway (dry and less snow cover). In southern Norway, permafrost is mostly associated with bedrock in mountain settings, with coarse ground moraines and regolith (Farbrot et al., 2013; Gisnås et al., 2013; 2017; Christiansen et al., 2010; Westermann et al., 2013) with the lower limit of discontinuous permafrost decreasing from c. 1600 m a.s.l. in the west to c. 1200 m a.s.l. in the east (Etzelmüller et al., 2003a). In northern Norway, on the other hand, the permafrost limit decreases from 800-900 m a.s.l. in the western mountains of Troms county, to 200-300 m a.s.l. in more continental areas, where it is often found in depressions characterized by peat plateaus (Borge et al., 2017).

The ongoing thawing and degradation of permafrost since the Little Ice Age (LIA) is likely to continue within the 21st century, with the lower altitudinal limit projected to rise up to 1800-1900 m a.s.l. in southern Norway (Hipp et al., 2012). Projections at the national scale based on an equilibrium model suggest that stable permafrost will be confined to 0.2% of mainland Norway by the end of the 21st century while it occupies about 6-6.5% of the ground at present, and was extending over 14% of the ground at the end of the LIA (Gisnås et al., 2013). At present, we can expect considerable areas in Norway with thawing and degrading permafrost, which at greater depths is likely also a transient response to post-LIA warming.

3 Methods

3.1 Rock surface temperature monitoring

During the summers of 2015 to 2017, twenty-one temperature loggers (Geoprecision, M-Log5W-ROCK) were installed in eight mountain areas to record RST at a depth of 10 cm with a 2-h interval (Fig. 1). The installation procedure followed the approach described by Gruber et al. (2004a). Together with the remaining four out of five temperature loggers installed in 2010 in Jotunheimen (Hipp et al., 2014), a network of twenty-five temperature loggers was available for this study. In order to represent a wide range of climate settings, they were distributed between 60.33° N and 69.46°N, 230 to 2320 m a.s.l., and in various aspects (Table 1, Fig. 2). Specific attention was paid to the topographical settings, to make sure that the loggers are not covered by snow during winter. This would make the recorded RST unsuitable for statistical modelling since it is unreliable to account for snow in such approaches. This is due to the high variability of snow in space and time in steep slopes, resulting from the interactions between topographical and topoclimatic factors controlling the snow thickness, distribution and thermal properties, and that produce highly fluctuating thermal effects (Haberkorn et al., 2015; 2017; Magnin et al., 2015a; 2017a).

3.2 Linear regression modelling and permafrost probability calculation

RST in steep slopes can be modelled by calculating the energy balance at the site (Gruber et al., 2004b), but for a regional survey with high spatial resolution, a statistical approach is better suited. From earlier investigations, it is widely accepted that RST is mainly related to incoming short-wave solar radiation and air temperature (Gruber

5 et al., 2004b, Hipp et al., 2014). These two parameters are easily obtained over larger regions and with sufficient spatial resolution, and thus available for multiple linear regression modelling. In a similar statistical approach, Boeckli et al. (2012a) have tested the role of precipitation and its seasonality, which have shown no significance.

In this study, we therefore predict the Mean Annual RST ($MARST_{pred}$) for the steep slopes of Norway as follows:

$$MARST_{pred} = a + PISR \times b + MAAT \times c \qquad (1)$$

10 where a is the $MARST_{pred}$ value when PISR and MAAT are equal to 0, PISR and MAAT are respectively the Potential Incoming Solar Radiation (PISR) and the Mean Annual Air Temperature (MAAT) at logger positions, with their respective coefficients b and c to be calculated. The model performance is assessed by the R^2, RMSE (Root Mean Square Error) and MAE (Mean Absolute Error), while the model residuals (measured MARST-$MARST_{pred}$) are used to evaluate the suitability of the data sample for the linear regression model. We further

15 performed a repeated ten-fold cross validation approach, which allows testing the model performance by partitioning the data set into ten sub-samples from which nine are used to fit the model while, one is kept to test the model (Gareth et al., 2014). The process is then repeated for each sub-sample and the means of the calculated $R2$, RMSE and MAE for each run are then provided to evaluate model performance (RM_{cv}, $RMSE_{cv}$ and MAE_{cv}). Ten folds balance the possible bias or high variability associated to respectively low and high fold numbers.

20 Finally, the probability of permafrost occurrence P(p) is expressed by the probability of $MARST_{pred}$ at a given location to be $\leq 0°C$. To calculate p, $MARST_{pred}$ is first transformed into a normal variable ($MARST_{norm}$) of mean $\mu = 0$ and variance $\sigma^2 = 1$ with:

$$MARST_{norm} = (-MARST_{pred} - \mu_{pred}) / \sigma_{pred} \qquad (2)$$

In which μ_{pred} and σ_{pred} are the mean and standard deviation of $MARST_{pred}$, respectively. The negative sign associated to $MARST_{pred}$ is necessary since we calculate the probability of $MARST_{pred}$ to be negative.

In the final step, p is calculated using a logistic approximation of the cumulative normal distribution developed by Bowling et al. (2009):

$$P(p) = \frac{1}{1+e^{-\left(0.07056 \times MARST_{norm}^{3} + 1.5976 \times MARST_{norm}\right)}} \qquad (3)$$

which ensures simplicity and accuracy in the permafrost probability calculation by guaranteeing a maximum

30 absolute error in probability < 0.00014 according to the comparison of Eq. (3) with the cumulative standard normal distribution (Bowling et al., 2009).

3.3 Calculation of model variables

In order to ensure the suitability of the collected RST time series for linear modelling, a visual preliminary data control is performed. Daily means are computed from hourly records and plotted against local air temperature (AT) measurements (Fig. 3). Smoothing of the temperature curves and disconnection with AT oscillations are

5   identified, since they indicate thick snow accumulation (Hanson and Hoelzle, 2004) which considerably influences the RST (Magnin et al., 2015a; Haberkorn et al., 2015: 2017). Daily RST data usually follows AT oscillations throughout the year (Fig. 3). In summer, the sensors, which are most exposed to solar radiation become warmer than both the air and the more shaded sensors. No obvious smoothing of the daily RST is found in the presented time series, making them all suitable for statistical modelling.

10   After this visual check, daily RST data are aggregated to mean annual values (MARST). For the eight loggers at Mannen, in Jotunheimen and in Alta, the records were interrupted by missing data. In order to calculate the MARST for the incomplete record the data gaps are filled by fitting a linear regression with local AT measurements (daily averages). For this, AT time series showing the best correlation with RST time series were chosen (Table 2). The RST data processing provides 85 MARST measurement points to fit the regression model.

15   MAAT for the measurement period is calculated for each MARST point, using local meteorological records at different elevations, from which a lapse rate is calculated. Similarly to the RST reconstruction, weather stations are chosen based on the best correlation between daily AT and RST records. To derive the most accurate MAAT during the RST measurement period, we calculate the lapse rate at a daily time step between relatively low- and relatively high-lying weather stations. When AT records are incomplete, an average lapse rate is calculated for

20   the period of the gap (two months overlap on each side of the gap) and for each of the recorded years. This yields a standard lapse rate value for the period of the gap, taking into account that lapse rate values can vary significantly throughout seasons. The meteorological data used to reconstruct MAAT at each of the MARST locations are presented in Table 3.

The PISR is then calculated for each MARST point at an hourly resolution over one year and considering a

25   transmissivity of 100% (no atmosphere) using the Spatial Analyst tools of ArcGIS (© ESRI, Redlands, CA, USA). PISR is highly sensitive to topographical settings (sun-exposure, slope and viewshed), and thus highly dependent on the quality and coverage of the DEM. For the Mannen, Narvik, Flåm, Loen and one of the Kåfjord (Gammanjunni) sites, 1 m resolution DEMs were available (Norge digital), while a 10 m resolution DEM (© Statens Kartverk, Norway) is available for entire Norway. The 1 m resolution DEMs only cover the relevant

30   summits and relief shading effects from the surrounding peaks is neglected in the PISR calculation. A sensitivity test based on the 10 m resolution DEM indicates that the relief shading effects are marginal on the summits, with maximal differences of 50 Wm^{-2}, while the effect of the resolution is crucial, especially close to the summits and ridges. This is due to the sharp topography which is hardly represented in medium-resolution DEM and can lead to differences ranging above 100 Wm^{-2}. We chose the PISR values to attribute to each MARST point by

35   averaging 3 to 5 pixel values best matching the measured topographical parameters (slope angle, aspect and

elevation), regardless of the DEM resolution since the slope angle and sun-exposure have a primary role compared to the relief shading effect. Results of the sensitivity analysis are provided in the Supplement together with the MARST, MAAT and PISR data used to fit the multiple linear regression model (Fig. S1, Tab. S1).

3.4 Permafrost mapping

5   MAAT and PISR are first mapped over the entire country based on the 10 m resolution DEM. The PISR is calculated using the same parameters as for the model explanatory variable: hourly time step and 100% transmissivity. The MAAT is mapped using the SeNorge2 dataset, which is interpolated from *in-situ* temperature observations over grid point elevations at 1 km resolution (Lussana et al., 2017), and daily AT grids available from 1957. For the downscaling to a 10 m resolution, we first averaged daily AT data of the normal period 1981-

10   2010 to generate a 1 km resolution MAAT raster. Then, for each 1 km grid cell, an average lapse rate is calculated over a radius of 25 km (Fig 5). This regional lapse rate is then used to interpolate 1km MAAT grid to a 10 m resolution. The 25 km radius ensures a precision at the regional scale, representing the relatively high lapse rate of the maritime coasts and the relatively low lapse rates in the more continental areas, while smoothing local patterns and possible artefacts.

15   MARST$_{pred}$ and permafrost probability are then mapped by implementing Eq. (1) and (3) in a raster calculator. Since the model is only valuable for steep slopes with restricted snow and debris covers, the map is only produced for slopes > 40°, which is a conservative threshold above which a 10 m resolution DEM is expected to display steep slopes.

3.5 Permafrost classes and interpretation keys

20   The permafrost probability is calculated as a continuous variable ranging from 0 to 1 which is then classified into four permafrost classes according to the international permafrost classification standards (Brown et al., 1997):

-    continuous permafrost for $p \geq 0.9$
-    discontinuous permafrost for $0.5 \leq p < 0.9$
-    sporadic permafrost for $0.1 \leq p < 0.5$
25   -   isolated permafrost is $p < 0.1$

Similarly to the Alpine-wide Permafrost Map covering the European Alps and its index interpretation keys (Boeckli et al., 2012b), the here proposed permafrost classes are interpreted against local bedrock settings (Fig. 5). Continuous permafrost suggests its existence in all conditions, regardless of the local settings. Discontinuous permafrost, the lower boundary of which corresponds to MARST$_{pred}$ = 0°C, suggests that it exists in most of the

30   rock faces, except those that are (sub-)vertical and compact. Generally fractured and rugged surfaces of steep bedrock slopes are characterized by colder conditions than unfractured and smooth bedrock surfaces. This is the

result of the effect of sparse snow deposits preventing from heating of direct solar radiation and the effect of air ventilation in fractures, which acts as a shortcut between the cold atmosphere and the subsurface (Hasler et al., 2011b; Magnin et al., 2015a; 2017a; Haberkorn et al., 2015). Sporadic permafrost suggests that permafrost exists only if the local settings are very favourable, meaning that the slope surface is substantially rugged and therefore

5   more significantly covered by snow and debris. Finally, isolated permafrost refers to isolated and perennial ice bodies found in open bedrock fractures at relatively low elevation.

4   Results

4.1   Model variables and summary statistics

10   The lowest MARST registered over the measurement period (Tab. 4) is found at Juv_4, the second highest measurement point, in 2012-2013, while the highest MARST is registered at Fla_S in 2017-2018, which is the most sun-exposed sensor installed at the lowest latitude. The minimum and maximum MAAT values are found at the highest and lowest measurement points, respectively: *i.e.* Juv_5 in 2010-2011 and Alt_S in 2016-2017. The lowest PISR value is at Fla_N, the most shaded sensor of the lowest latitude, and the highest one is at Adj_S, a high-elevated and south-exposed logger in northern Norway (Fig. 5).

15   At eleven loggers, the measurements directly suggest permafrost occurrence (negative MARST every year). Permafrost-free conditions (positive MARST every year) are suggested at nine loggers with recorded MARST consistently > 1°C, and possible permafrost, with MARST oscillating between -1 and 1.5°C is found at 5 loggers. The presence of permafrost is nevertheless not excluded where positive MARSTs are recorded, because of the transient effect at depth from former colder periods (Noetzli and Gruber, 2009; Myhra et al., 2017), and a

20   possible temperature offset (*i.e.* temperature difference between the surface and depth) resulting from the fracturing and snow deposits (Hasler et al., 2011b).

The MARST difference between north-exposed and south-exposed faces is around 3.5°C in southern Norway (*e.g.* 3.5°C at Fla_S and 0.2°C at Fla_N in 2017-2018), while it is around 1.5°C in northern Norway (*e.g.* 0.2°C at Adj_S and -1.4°C at Adj_N in 2015-2016). This difference between northern and southern Norway coincides

25   with higher PISR values at north-exposed slopes of northern Norway, with for example 100 W.m^{-2} more at Adj_N or Gam_N than at Fla_N or Man_N.

Table 5 summarizes the statistics of the regression model. For most of the measurement points, the MARST is generally higher than the MAAT (Fig. 6a) and the difference between MARST and MAAT (surface offset) increases with increasing PISR (Fig. 6b), confirming previous studies of steep bedrock thermal characteristics

30   (Boeckli et al., 2012a; Magnin et al., 2015a). The surface offset ranges from 0 to 4°C, the highest values being found at the most sun-exposed sites (Fig. 6b). In some rare cases, the MARST is sligthly lower than the MAAT (Fig. 6a), which indicates possible local factors cooling the most shaded rock faces (wind or ice for example). An

increase of 100 W.m^{-2} induces an increase of about 1°C in MARST and is equivalent to an increase of 1°C in MAAT. The adjusted R^2, RMSE and MAE demonstrate the good fit of the model, which is corroborated by the consistency of these values with those of the R$^2_{cv}$, RMSE$_{cv}$ and MAE$_{cv}$ (Tab. 5) from our cross-validation procedure. The model residuals confirm that the data sample is well suited for the chosen statistical approach (Fig. 7): they are randomly distributed around 0°C, and no noticeable outlier is detected.

4.2 Permafrost distribution in steep slopes

Steep slopes represent almost 2% of the surface area of mainland Norway, constituting about 7300 km^2 between sea level and 2460 m a.s.l. (surface area covered by slopes >40° on the 10 m resolution DEM). The rock wall surface area is unequally distributed across latitudes with almost 20% lying between 61 and 62°N (Fig. 8a), where the highest peaks of Norway are located (Fig. 8b). West-facing slopes are generally predominant (30%), while south-exposed faces are less frequent (20%), and north and east facing-slopes each represent a quarter of the steep slope surface area. However, this global pattern is not constant across latitudes, with for example, predominantly north-facing slopes between 65 and 67°N (Fig. 8a).

Continuous permafrost occupies about 2% of the rock wall surface area, discontinuous permafrost about 9% and sporadic permafrost about 20%, meaning that 31% of the rock wall surface area features a permafrost probability ≥ 0.1 and 11% a probability ≥ 0.5. In the southernmost part of Norway (58°N), sparse occurrences of sporadic permafrost are found as low as 830 m a.s.l. in all aspects, except south (Fig. 9). Discontinuous permafrost occurs from 59°N with the lowermost observations of the lower altitudinal limit (LAL) at 1150 m a.s.l. in north faces, and 50% of the LAL observations above 1300-1400 m a.s.l.. At the same latitude, sparse occurrences of continuous permafrost are found from 1700 m a.s.l. in north and east faces. Continuous permafrost is more widespread at 61 and 62°N, in accordance with rock wall frequency and elevation. The 1st quartile of the observations of LAL of continuous permafrost is around 1500 m a.s.l. in north faces, 1700 m a.s.l. in east and west faces, and 1900 m in south faces. Little permafrost is found in the steep bedrock slopes between 63 and 65°N, concordant with rock-wall frequency and elevation. From 67 to 69°N, continuous permafrost exists mostly above 1100 m a.s.l. in north faces, 1200 m a.s.l. in east and west faces, and 1400 m a.s.l. in south faces. The LAL for discontinuous permafrost decreases from 900 to 700 m a.s.l. in north faces, over 800-900 m a.s.l. for east and west faces, and down to 1000 m a.s.l. for south faces between 67 and 69°N. Sparse occurrences of discontinuous permafrost are found as low as 50 m a.s.l. in all aspects at 69 and 70°N. At 70°N, the highest permafrost probability is 0.9, meaning that continuous permafrost is mostly absent, mainly because the elevation of rock walls rarely exceed 1000 m a.s.l..

The medians of observations of the LAL of each permafrost class decrease by about 500±50 m from southern to northern Norway, decreasing by about 50 m with every degree northwards for north facing slopes, and with 58 m for the south facing slopes. For example, the median of the observations of the LAL of discontinuous permafrost at 60°N is at 1210 m a.s.l. and 1580 m a.s.l. in the north and south faces respectively, and at 760 m a.s.l. and 1060 m a.s.l. at 69°N. In southern Norway, permafrost therefore exists 350 to 400 m lower in north faces

compared to south faces, while it is 200 to 250 m lower in northern Norway. These decreases in the LAL of permafrost classes according to latitude and aspect do not appear linear (Fig. 9) because the rock-wall distribution significantly controls this relationship (Fig. 8). However, there is a high correlation between the distribution of the 0°C isotherm (lower limit of discontinuous permafrost) and latitude (Fig. 10). The lower limit

5 of permafrost decreases by about 60 m every degree northwards for north faces and almost 70 m for south facing slopes.

The number of permafrost observations decreases with continentality (Fig. 10) as most of the rock walls are found in the Caledonides close to the coast and in the interior mountain massifs of southern Norway such as Jotunheimen, Rondane or Dovrefjell (Fig. 11). In relation to continentality, the decrease in observations makes a

10 statistical analysis of permafrost distribution poorly relevant. Nevertheless, we note that the lowermost occurrences of discontinuous permafrost in north faces of southern Norway are found at the furthest distance from the sea, in Sølen, Sennsjøkampen, and the border with Sweden in the Nesjøen area (Fig. 10 and 11). In northern Norway, the lowermost occurrences of discontinuous permafrost are not found near the coast, but further inland (about 25 to 50 km away from the sea, Fig. 11). At such distance, low-elevated rock walls (< 200

15 m a.s.sl.) are mostly found in river canyons, such as at the Alta, Reisa or Tana rivers (Fig. 11). It is also noteworthy that in the general, the dominant areas of permafrost rock walls are located west of the main distribution of permafrost in Norway according to *e.g.* Gisnås et al. (2017).

5   Discussion

5.1 Model evaluation

20 To evaluate the permafrost probability model, we compare the permafrost probability map for the steep slopes of Norway, named "CryoWall map" in the following, to the rare permafrost evidences and studies in steep slopes of Norway. Unlike gentle slope permafrost, which produces typical landforms, such as rock glaciers or palsas and peat plateaus, permafrost in steep slopes only becomes evident by ice in rock fractures or failure scars. In northern Norway, Blikra and Christiansen (2014) observed sporadic permafrost in the fractures of the Jettan rock

25 slide, extending from 400 to 800 m a.s.l., which is corroborated by the CryoWall map (Fig. 11 and 12a). About 45 km southwest of Jettan, a 500,000 m^3, in June 2008, rock mass detached from the East face of Polvartiden (1275 m a.s.l.), from an elevation of 600 m a.s.l., uncovering ice in the scar. Frauenfelder et al., (2018) simulated permafrost in the Polvartinden summit by mean of 2D numerical modelling tools based on several years of rock wall temperature information. These simulations estimated a lower limit of permafrost (0°C isotherm) at about

30 650 m, which is the top of the rock slope failure and the lower limit of discontinuous permafrost suggested by the CryoWall map (Fig. 12b).

In southern Norway, Etzelmüller et al. (2003b) report that ice was found during construction work in the 1950s at about 1500-1600 m in the bedrock of Gaustatoppen (1883 m a.s.l.), where the CryoWall map indicates discontinuous permafrost (Fig. 12c). Gaustatoppen is made of Precambrian quartzite, prone to macrogelivation

and therefore to the producing of geometric blocks (Sellier, 1995). Combined with slopes rarely exceeding 55°, this results in a significant debris cover, favouring snow accumulation in winter and permafrost persistence, even with a relatively low probability value. Protruding rock outcrops also exists at Gaustatoppen, but they are generally highly fractured and covered by thin snow in winter, which makes them also favourable to permafrost persistence.

In relation to the study by Steiger et al. (2016), this approach is an improvement as (i) we calibrate our model with observations and therefore account for the important influence of topographic aspect, (ii) we use an updated and improved spatial interpolation method for 2 m AT that has been used to build the SeNorge2 dataset (Lussana *et al.* 2017), (iii) we downscale AT using a regional lapse rate instead of using a standard and uniform one. The main pattern of steep-slope permafrost distribution is comparable, while locally deviations related to sun-exposure are substantial. For example, Steiger et al. (2016) suggested a lower limit of rock wall permafrost around 850 m a.s.l. in the Lyngen Alps, which is the limit of the third quartile of the observations of the LAL of discontinuous permafrost in north faces, and below the first quartile of these observations in the north faces (Fig. 15). Steiger et al. (2016) also found a lower limit of rock wall permafrost close to sea level in the Varanger Peninsula (70°N) while the CryoWall map suggests discontinuous permafrost above 100 m a.s.l. only (Fig. 15).

Comparison with results from Myhra et al. (2017) who modelled permafrost distribution and evolution since the LIA for four sites of Norway is limited because of the idealized test cases considered in this study, which do not account for local topographical characteristics and insolation. A comparative figure of the CryoWall map and Myhra et al. (2017) models is provided in the Supplement (Fig. S2).

5.2 Permafrost characteristics in the steep slopes of Norway compared to other areas

Permafrost affecting steep rock slopes has mostly been studied in rock walls of the European Alps (45-46°N), where the lower limit of the isotherm 0°C lies around 2800±300 m a.s.l. in north faces and 3800±300 m a.s.l. in south faces (Gruber et al., 2004a; 2004b; Magnin et al., 2015b). This difference of about 1000 m elevation between north and south faces is directly imputed to the solar radiation control, which results in a MARST difference reaching 8°C between the north and south faces of a same elevation. In British Columbia (Canada), north faces are 4°C colder than south faces between 54°N and 59°N (Hasler et al., 2015). In the southern Alps of New Zealand, at 43°S, differences between north and south faces reaching a maximum of 5°C were reported (Allen et al., 2009). Our study presents MARST measurements at higher latitudes, where smaller and decreasing north-south differences with latitude are observed. This is the result of less and more direct solar radiation in south and north-facing slopes, respectively, which is reinforced at higher latitude due to the polar night in winter and midnight sun during summer. This also explains the decreasing difference between the LAL limit of south and north faces towards lower latitudes (Fig. 9), where the south faces receive more solar radiation, unbalancing the air temperature controls, while the north facing slopes receive less direct solar radiation and are more directly controlled by air temperature.

Despite the solar radiation control, which seems to be predominant in the RST patterns from local to continental scales, additional factors may also affect the RST. The snow that accumulate in various thicknesses in steep slopes has been recognized as a significant factor affecting the RST at the local scale, as it attenuate both, the winter cooling (Haberkorn et al., 2017) and the insolation heating in late winter and spring (Magnin et al.,

5   2017b). In Norway, snow and frost coating (mainly due to atmospheric icing, *i.e.* high elevation rock walls that are exposed to supercooled water in clouds and if combined with strong wind it can produce heavy ice accretions) are common in some of the high-elevation areas, and can provoke significant inter-annual variability of MARST in prevailing wind direction and preferential snow deposition (Frauenfelder et al. 2018). Furthermore, energy exchanges due to latent and sensible heat effects that are relatively more important in high-latitude and maritime

10   settings than in more continental mountain areas possibly affect the RST patterns. In the same way, cloudiness, that is generally more important in maritime settings, may also play an important role. This is evidenced by the relatively small north-south difference in the southern Alps of New Zealand that are at a rather low latitude but famous for their high precipitation rates. Such effects are not easily detectable by mean of visual control or statistical analysis and point out the need for more physic-based investigations in order to better understand their

15   respective influence on MARST patterns and permafrost distribution. However, the good fit of observations with the simple linear model indicates that such effects are only of minor relevance for Norway and do not strongly affect the overall permafrost distribution in steep slopes.

5.3 Permafrost characteristics in the steep slopes compared to other permafrost terrains in Norway

The distribution of permafrost has been estimated in various regions of southern and northern Norway by means

20   of Bottom temperature of snow cover (BTS) measurements (Haeberli, 1973), rock glacier inventories, ground temperature monitoring, geophysical soundings and numerical models.

In central southern Norway, the LAL of gentle slope permafrost decreases with continentality, being at c. 1500 m a.s.l. in Jotunheimen (Isaksen et al., 2002; Farbrot et al., 2011), down to 1300 m a.s.l. in Dovrefjell at sites with no snow cover (Sollid et al., 2003; Isaksen et al., 2011; Westermann et al., 2013), and 1100 m a.s.l. in more

25   eastern continental terrains in the Femunden region with a thin snow cover (Heggem et al., 2005; Westermann et al., 2013; Gisnås et al., 2017). The CryoWall map confirms this decreasing elevation of the lower limit of permafrost across continentality (Fig. 10 and 13). However, the LAL of permafrost in gentle slopes of Jotunheimen is close to the LAL of permafrost in south-facing rock walls, but 300-400 m higher than in the north-facing rock walls (Fig. 13). At the local scale, the transition between continuous and discontinuous

30   permafrost is similar in north-exposed rock walls than in gentle slopes, while discontinuous permafrost in south-exposed rock-walls rather occurs in the continuous permafrost zone of for the surrounding gentle slopes (Fig. S3a). In Dovrefjell further east, the LAL in gentle slopes rather corresponds to the lower LAL of north-exposed rock walls, while it is about 200-300 m lower than in south-exposed rock walls. But at the local scale, the transition between continuous, discontinuous and sporadic permafrost coincides remarkably well to the map

35   based on BTS measurement (Isaksen et al., 2002) produced by Etzelmüller (unpublished), even for south-exposed rock walls (Fig. S3b). In eastern Norway, rock faces are rare and therefore evidences of permafrost

distribution is steep bedrock slopes are sparse. However, discontinuous permafrost is found as low as 960 m a.s.l. in the north face of Sennsjøkampen, and above 1290 m a.s.l. in south, east and west faces of Sølen (Fig. 13). This is generally higher than in surrounding slopes where permafrost generally occurs at much lower elevation (Heggem et al., 2005; Fig. S3c).

5   In northern Norway, the lower limit of permafrost in gentle slopes and flat terrains lies around 800-900 m a.s.l. in the coastal mountains of Troms county, such as in the Lyngen Alps (Farbrot et al., 2013, Steiger et al 2016), and decreases to 300-500 m a.s.l. in the coastal areas and mires in the inner part of Finnmark (Isaksen et al., 2008; Farbrot et al., 2013; Borge et al., 2017). In the interior part of the Varanger peninsula the lower limit of permafrost in gentle slopes and flat terrains is around 400-450 m a.s.l. (Isaksen et al. 2008). Observations in the
10   steep slopes of the Varanger peninsula (Fig. 13) show, that permafrost can occur at lower elevations than in gentle slopes in coastal Finnmark. The only rock faces existing in the inner part of Finnmark are mostly the river canyons, where discontinuous permafrost occurs between 100 and 600 m a.s.l. (Fig. 10 and 11), favoured by the high confinement and resulting low solar radiation input. The occurrence of permafrost may be underestimated in some places of continental areas due to local temperature inversion which are smoothed by the regional lapse
15   rate calculation (e.g. Fig. 4).

5.4 Implications for landscape development in Norway

The CryoWall map confirms most of the previous findings in terms of permafrost occurrence and distribution in steep slopes inferred from visible ice or numerical modelling experiments. It is therefore a reliable basis to assess rock wall permafrost in Norway. The collected RST time series and CryoWall map may be used to model the
20   permafrost evolution through time, using the predicted MARST or the measured RST as upper boundary conditions for 1D or 2D simulation (Hipp et al., 2014; Magnin et al., 2017b). The permafrost models and the CryoWall map supports investigations on large-scale rock slope deformations, slope hazards such as rock falls and the assessment of geomorphological processes. To illustrate some of the research problems our map can contribute, we give some examples and analysis in the following.

25   *Large-scale rock slope deformations in Norway* – In the Norwegian mountains numerous sites, with large scale instabilities are identified through systematic mapping and surveillance during the last years (*e.g.* Hermanns et al., 2012; Bunkholt et al., 2013; Oppikofer et al., 2015). Seven sites comprise a high hazard level, justifying installation of an early warning system, two of which have been equipped with RST loggers in this study. We now used the CryoWall map to assess permafrost occurrence at "critical slopes" inventoried by the Geological
30   Survey of Norway (Oppikofer et al., 2015, http://geo.ngu.no/kart/ustabilefjellparti_mobil/). The database comprises unstable slopes (postglacial deformation that could lead to catastrophic slope failures), deformed rock slopes that can produce rock falls, potential unstable slopes (that match the structural inventory for failure but have no signs of deformation), and morphological lineaments along steep slopes that are the result of erosional processes. Each critical slope is recorded as a point at about the middle of the slope. To extract permafrost
35   probability at this point and overcome limitations related to the mismatch between the location of steep areas in

the respective slopes and the location of the points, we created a buffer of 200 m around each point to ensure that the point surface areas cover most of the slope, including the steep parts. The maximum permafrost probability contained in the buffer area of each point was then extracted for 1339 registered critical slopes, and 11% of them are permafrost slopes (probability > 0.5). The distribution of these critical slopes is displayed in the Supplement

5   (Fig. S4). This preliminary investigation points out the critical slopes that may deserve further investigations on the potential role of permafrost in their ongoing or possibly future destabilization, especially in the current context of climate change and permafrost degradation. As a further step, the hazard level could be statistically linked to the permafrost probability following a similar approach as the one conducted by (Ravanel et al., 2017) in the Mont Blanc massif.

10   *Periglacial geomorphology* - Rock glaciers and stable ice-cored moraines are the only landforms directly indicating permafrost presence in mountain regions (e.g. Berthling ,2011, Haeberli 2000, Etzelmüller and Hagen 2005. These landforms are normally associated to steep slopes, at least in the vicinity. We used a rock glacier/stable ice-cored moraine inventory for Norway (Lilleøren and Etzelmuller, 2011) and compared adjacent rock walls of active rock glaciers to our results. We found that most rock walls associated to active rock glaciers

15   or to cirques where ice-cored moraines emerge, were classified as discontinuous to continuous permafrost, at least in their upper part (Fig. S5). This underpins the interest for studying the connection of permafrost rock walls and adjacent landforms which so far, to the author's knowledge, has not been directly addressed. Indeed, permafrost dynamics can influence material supply pattern to these landforms, as e.g. frost cracking varies greatly within and without permafrost environments (e.g. Hales and Roering, 2007).

20   *Landscape development* - It is evident that the understanding of thermal regime within mountain slopes, and its development during past and the future, has a geomorphological relevance (Berthling and Etzelmuller, 2011, Hales and Roering, 2007). Frost weathering and stabilisation/destabilisation of slopes over long time scales due to climate variability and glaciation cycles work in concert, and in certain temperature bands. For example, the frost cracking window (e.g. Hallet et al., 1991; Hales and Roering, 2007) defines a narrow temperature band, in

25   which frost weathering processes are most effective, resulting in ice segregation and subsequent rock falls. On the other hand, deep permafrost aggradation/degradation weakens rock masses, with the possibility of larger-scale slope destabilisation on longer time scales (e.g. Krautblatter et al., 2013). Moreover, steep rock walls, often snow free or with little snow cover can influence the thermal regime of adjacent areas due to lateral heat flux (Myhra et al., 2017), with the possibility to maintain large temperature gradients. All these processes influences

30   material predication and erosion of mountain ranges and contribute to the periglacial realm being an important environment for weathering (Hales and Roering 2007), valley formation (Büdel, 1981 and landscape planation ("periglacial buzzsaw") (e.g. Egholm et al., 2015).

Finally, the collected RST time series may be used for a detailed analysis of RST patterns over different environmental settings (climate, topography), and support the development of a possible and straightforward

35   model of rock wall permafrost distribution at the continental scale (Sect. 5.2). This would require a systematic sampling of steep slopes to ensure their representativeness of idealized case directly coupled with the atmosphere

and no specific topographical settings affecting their insolation, as well as further investigations on the atmospheric moisture and cloudiness controls.

6   Conclusions

From this study the following main conclusions can be drawn:

- Sporadic permafrost occupies about 20 % of the steep slope surface area in mainland Norway. It can be found as low as 830 m a.s.l. in north faces at 59°N and down to sea level in all aspect in northern Norway.

- Discontinuous permafrost occupies 9% of the rock wall surface area and can be found in southern Norway (from 59°N) mostly above 1300-1400 m a.s.l. in north faces and 1600-1700 in south faces. In northern Norway, it mainly occurs above 750 m a.s.l. in north faces and 1050 m a.s.l. in south faces.

- Continuous permafrost occupies 2% of the rock wall surface area between 59°N and 69°N, with substantial presence above 1500 m a.s.l. in north faces and 1900 m a.s.l. in south faces of southern

Norway. In northern Norway, it is widespread above 1100 m a.s.l. in north faces, and 1400 m a.s.l. in south faces.

- The difference in mean annual rock surface temperature of north and south facing slopes at similar elevation is about 3.5°C in southern Norway and 1.5°C in northern Norway due to the effect of solar radiation in relation with the polar night/midnight sun effect at higher latitudes. The differences are

substantially lower than in reported alpine areas of lower latitudes.

- The lower elevation limit of permafrost decreases by about 500±50 for between southern and northern Norway, with a more pronounced decrease for south-exposed slopes (-50m for every degree northwards for north-exposed slopes against -58 m for the south-exposed ones).

- The lower elevation limit of permafrost also decreases across continentality, with occurrences of

discontinuous permafrost about 200 m lower in eastern Norway than in the west coast of southern Norway, and below 200 m a.s.l. in the river canyons of northern Norway.

- Steep slope permafrost generally occurs lower than in gentle mountain slopes in north faces, but at higher elevation in south faces. This pattern is nevertheless more or less pronounced depending on the regions of Norway.

Data availability
The CryoWall map will be made available after publication via the NIRD research data archive: https://archive.norstore.no/

Authors contributions
FM led the preparation of the manuscript with guidance from BE, and input from SW, KI, PH and RH. The
35
overall research project was conducted by BE with significant contributions from other authors. FM, BE, PH and

Acknowledgement

This study is part of the CryoWALL project (243784/CLE) funded by the Research Council of Norway (RCN).
5   Additional funding, both directly or indirectly, was provided by the University of Oslo, the Norwegian Geological Survey and the Norwegian Water and Energy Directorate (NVE). Bas Altena, Thorben Dunse, Justyna Czekirda, Jaroslav Obu, Ove Brynildsvold (all University of Oslo), Joel Fiddes (SLF, Switzerland), Amund Mundhjeld (Raubergstulen) and Solveig Winsvold (NVE) helped with either installing rock wall loggers or reading them out. C. Lussana (Meteorological Institute of Norway) guided the processing of the SeNorge2
10 dataset. We especially thank NVE, section for rock slide early warning ("Fjellskredovervaking") and its leader, Lars Harald Blikra, both in Stranda and in Kåfjord, Troms, for their enthusiastic support during field work and later discussions. We want to thank all mentioned individuals and institutions.

References

15 Allen, S. K., Gruber, S. and Owens, I. F.: Exploring steep bedrock permafrost and its relationship with recent slope failures in the Southern Alps of New Zealand, Permafrost and Periglacial Processes, 20(4), 345–356, doi:10.1002/ppp.658, 2009.

Ballantyne, C. K.: Paraglacial geomorphology, Quaternary Science Reviews, 21(18), 1935–2017, doi:10.1016/S0277-3791(02)00005-7, 2002.

Berthling, I., and Etzelmüller, B.: The concept of cryo-conditioning in landscape evolution. Quaternary Research, 20 75(2), 378-384, 2011.

Blikra, L. H. and Christiansen, H. H.: A field-based model of permafrost-controlled rockslide deformation in northern Norway, Geomorphology, 208, 34–49, doi:10.1016/j.geomorph.2013.11.014, 2014.

Boeckli, L., Brenning, A., Gruber, S. and Noetzli, J.: A statistical approach to modelling permafrost distribution in the European Alps or similar mountain ranges, The Cryosphere, 6(1), 125–140, doi:10.5194/tc-6-125-2012,
25 2012a.

Boeckli, L., Brenning, A., Gruber, S. and Noetzli, J.: Permafrost distribution in the European Alps: calculation and evaluation of an index map and summary statistics, The Cryosphere, 6(4), 807–820, doi:10.5194/tc-6-807-2012, 2012b.

Bohme, M., Oppikofer, T., Longva, O., Jaboyedoff, M., Hermanns, R. L., and Derron, M.-H.: Analyses of past
30 and present rock slope instabilities in a fjord valley: Implications for hazard estimations, Geomorphology, 248: 464–474, 2015.

Borge, A. F., Westermann, S., Solheim, I. and Etzelmüller, B.: Strong degradation of palsas and peat plateaus in northern Norway during the last 60 years, The Cryosphere, 11(1), 1–16, doi:https://doi.org/10.5194/tc-11-1-2017,
35 2017.

Bowling, S. R., Khasawneh, M. T., Kaewkuekool, S. and Cho, B. R.: A logistic approximation to the cumulative normal distribution, Journal of Industrial Engineering and Management, 2(1), 114–127, doi:10.3926/jiem..v2n1.p114-127, 2009.

Brown J, Ferrians OJ, Heginbottom JA, Melnikov ES. 1997. International Permafrost Association Circum-Arctic
40 Map of Permafrost and Ground Ice Conditions, Map CP-45. US Geological Survey.

Büdel, J. Klima-geomorphologie. 304 pp, Gebrüder Bornträger, Berlin, ISBN 978-3-443-01017-1, 1981.

Bunkholt, H., Nordahl, B., Hermanns, R. L., Oppikofer, T., Fischer, L., Blikra, L. H., Anda, E., Dahle, H., and Sætre, S. Database of unstable rock slopes of Norway. In C Margottini, P Canuti and K Sassa (eds.), *Landslide science and practice*, 423–428, Springer, Berlin, Heidelberg, 2013.

Christiansen, H. H., Etzelmüller, B., Isaksen, K., Juliussen, H., Farbrot, H., Humlum, O., Johansson, M., Ingeman-Nielsen, T., Kristensen, L., Hjort, J., Holmlund, P., Sannel, A. B. K., Sigsgaard, C., Åkerman, J., Foged, N., Blirka, L. H., Pernosky, M. A. and Ødegård, R. S.: The thermal state of permafrost in the nordic area during the international polar year 2007–2009, [online] Available from: https://onlinelibrary.wiley.com/doi/10.1002/ppp.687 (Accessed 12 November 2018), 2010.

Davies, M. C. R., Hamza, O. and Harris, C.: The effect of rise in mean annual temperature on the stability of rock slopes containing ice-filled discontinuities, Permafrost and Periglacial Processes, 12(1), 137–144, doi:10.1002/ppp.378, 2001.

Deline, P., Gruber, S., Delaloye, R., Fischer, L., Geertsema, M., Giardino, M., Hasler, A., Kirkbride, M., Krautblatter, M., Magnin, F., McColl, S., Ravanel, L., and Schoeneich. P.: Ice Loss and Slope Stability in High-Mountain Regions In: Snow and Ice-Related Hazards, Risks and Disasters http://dx.doi.org/10.1016/B978-0-12-394849-6.00015-9, 2015.

Egholm, D. L., Andersen, J. L., Knudsen, M. F., Jansen, J. D., and Nielsen, S. B.: The periglacial engine of mountain erosion-Part 2: Modelling large-scale landscape evolution. Earth Surface Dynamics, 3(4), 2015.

Etzelmüller, B, Berthling, I, Sollid, J. L.: Aspects and concepts on the geomorphological significance of Holocene permafrost in southern Norway, Geomorphology, 52, 87-104. DOI:10.1016/s0169-555x(02)00250-7, 2003a.

Etzelmüller, B., Berthling, I., and Ødeg°ard, R.: 1-D-DC-resistivity depth soundings in high mountain areas of Southern Norway – a tool in permafrost investigations, Z. Geomorph., Suppl. Bind, 32, 19–36, 2003b.

Etzelmuller, B., Romstad, B., and Fjellanger, J.: Automatic regional classification of topography in Norway: Norwegian Journal of Geology - Norsk Geologisk Tidsskrift, v. 87, p. 167-180, 2007.

Farbrot, H., Hipp, T. F., Etzelmüller, B., Isaksen, K., Ødegård, R. S., Schuler, T. V. and Humlum, O.: Air and Ground Temperature Variations Observed along Elevation and Continentality Gradients in Southern Norway - Farbrot - 2011 - Permafrost and Periglacial Processes - Wiley Online Library, [online] Available from: https://onlinelibrary.wiley.com/doi/full/10.1002/ppp.733 (Accessed 12 November 2018), 2011.

Farbrot, H., Isaksen, K., Etzelmüller, B. and Gisnås, K.: Ground Thermal Regime and Permafrost Distribution under a Changing Climate in Northern Norway, [online] Available from: https://onlinelibrary.wiley.com/doi/full/10.1002/ppp.1763 (Accessed 12 November 2018), 2013.

Fischer, L., Kääb, A., Huggel, C. and Noetzli, J.: Geology, glacier retreat and permafrost degradation as controlling factors of slope instabilities in a high-mountain rock wall: the Monte Rosa east face, Natural Hazards and Earth System Sciences, 6(5), 761–772, doi:https://doi.org/10.5194/nhess-6-761-2006, 2006.

Fischer, L., Amann, F., Moore, J. R. and Huggel, C.: Assessment of periglacial slope stability for the 1988 Tschierva rock avalanche (Piz Morteratsch, Switzerland), Eng Geol, 116(1–2), 32–43, doi:10.1016/j.enggeo.2010.07.005, 2010.

Frauenfelder, R., Isaksen, K., Lato, M. J. and Noetzli, J.: Ground thermal and geomechanical conditions in a permafrost-affected high-latitude rock avalanche site (Polvartinden, northern Norway), The Cryosphere, 12(4), 1531–1550, doi:https://doi.org/10.5194/tc-12-1531-2018, 2018.

Furseth, A.: Skredulykker i norge, Tun Forlag, Oslo, Norway, 207 pp, 2006.

Gareth, J. Witten, D., Hastie, T., and Tibshirani, R.: An Introduction to Statistical Learning: With Applications in R. Springer Publishing Company, Incorporated, 426 p, 2014.

Gisnås, K., Etzelmüller, B., Schuler, T. V. and Westermann, S.: CryoGRID 1.0: Permafrost Distribution in Norway estimated by a Spatial Numerical Model, [online] Available from: https://onlinelibrary.wiley.com/doi/full/10.1002/ppp.1765 (Accessed 12 November 2018), 2013.

Gisnås, K., Westermann, S., Schuler, T. V., Melvold, K., Etzelmüller, B.: Small scale variation of snow in a regional permafrost model, The Cryosphere, 10, 1201–1215, DOI:10.5194/tc-10-1201-2016, 2016.

Gisnås, K., Etzelmüller, B., Lussana, C., Hjort, J., Sannel, A. B. K., Isaksen, K., Westermann, S., Kuhry, P., Christiansen, H. H., Frampton, A. and Åkerman, J.: Permafrost Map for Norway, Sweden and Finland, Permafrost and Periglacial Processes, 28(2), 359–378, doi:10.1002/ppp.1922, 2017.

5   Gruber, S., Hoelzle, M. and Haeberli, W.: Permafrost thaw and destabilization of Alpine rock walls in the hot summer of 2003 - Gruber - 2004 - Geophysical Research Letters - Wiley Online Library, [online] Available from: https://agupubs.onlinelibrary.wiley.com/doi/full/10.1029/2004GL020051 (Accessed 12 November 2018a), 2004.

Gruber, S., Hoelzle, M. and Haeberli, W.: Rock-wall temperatures in the Alps: modelling their topographic distribution and regional differences, Permafrost and Periglacial Processes, 15(3), 299–307, doi:10.1002/ppp.501, 2004b.

10   Haberkorn, A., Phillips, M., Kenner, R., Rhyner, H., Bavay, M., Galos, S. P. and Hoelzle, M.: Thermal regime of rock and its relation to snow cover in steep alpine rock walls: Gemsstock, Central Swiss Alps, Geografiska Annaler Series A: Physical Geography, 97(3), 579–597, doi:10.1111/geoa.12101, 2015.

Haberkorn, A., Wever, N., Hoelzle, M., Phillips, M., Kenner, R., Bavay, M., and Lehning, M.: Distributed snow and rock temperature modelling in steep rock walls using Alpine3D, The Cryosphere, 11, 585-607,
15   https://doi.org/10.5194/tc-11-585-2017, 2017.

Haeberli, W. Die Basis-Temperatur der winter-lichen Schneedecke als moglicher Indikator fur die Verbreitung von Permafrost in den Alpen. Zeitschrift fur Gletscherkunde und Glazialgeologie, 9, 221-227, 1973.

Haeberli, W., Huggel, C., Kääb, A., Zgraggen-Oswald, S., Polkvoj, A., Galushkin, I., Zotikov, I. and Osokin, N.: The Kolka-Karmadon rock/ice slide of 20 September 2002: an extraordinary event of historical dimensions in
20   North Ossetia, Russian Caucasus, Journal of Glaciology, 50(171), 533–546, doi:10.3189/172756504781829710, 2004.

Hales, T. C., and Roering, J. J.: Climatic controls on frost cracking and implications for the evolution of bedrock landscapes. Journal of Geophysical Research: Earth Surface, 112(F2), 2007.

Hallet, B., J. Walder, and Stubbs, C. W.: Weathering by segregation ice growth in microcracks at sustained sub-
25   zero temperatures: Verification from an experimental study using acoustic emissions, Permafrost Periglacial Processes, 2, 283– 300, 1991.

Hanson, S. and Hoelzle, M.: The thermal regime of the active layer at the Murtèl rock glacier based on data from 2002, Permafrost and Periglacial Processes, 15(3), 273–282, doi:10.1002/ppp.499, 2004.

Harris, C., Haeberli, W., Mühll, D. V. and King, L.: Permafrost monitoring in the high mountains of Europe: the
30   PACE Project in its global context, Permafrost and Periglacial Processes, 12(1), 3–11, doi:10.1002/ppp.377, 2001.

Hasler, A., Gruber, S., Font, M. and Dubois, A.: Advective Heat Transport in Frozen Rock Clefts: Conceptual Model, Laboratory Experiments and Numerical Simulation, Permafrost and Periglacial Processes, 22(4), 378–389, doi:10.1002/ppp.737, 2011a.

35   Hasler, A., Gruber, S. and Haeberli, W.: Temperature variability and offset in steep alpine rock and ice faces, The Cryosphere, 5(4), 977–988, doi:10.5194/tc-5-977-2011, 2011b.

Hasler, A., Geertsema, M., Foord, V., Gruber, S. and Noetzli, J.: The influence of surface characteristics, topography and continentality on mountain permafrost in British Columbia, The Cryosphere, 9(3), 1025–1038, doi:https://doi.org/10.5194/tc-9-1025-2015, 2015.

40   Heggem, E. S., Juliussen, H. and Etzelmüller, B.: Mountain permafrost in Central-Eastern Norway, Norsk Geografisk Tidsskrift - Norwegian Journal of Geography, 59(2), 94–108, doi:10.1080/00291950510038377, 2005.

Hermanns, R., Hansen, L., Sletten, K., Böhme, M., Bunkholt, H., Dehls, J., Eilertsen, R., Fischer, L., L'Heureux, J.-S., Høgaas, F., Nordahl, B., Oppikofer, T., Rubensdotter, L., Solberg, I.-L., Stalsberg, K., and Molina, F. X.
45   Y.: Systematic geological mapping for landslide understanding in the Norwegian context, Landslide and

engineered slopes: protecting society through improved understanding, Taylor & Francis Group, London: 265-271, 2012.

Hermanns, R.L., Dahle, H., Bjerke, P.L., Crosta, G.B., Anda, E., Blikra, L.H., Saintot, A., Longva, O., Eiken, T.: Rock slide dams in Møre og Romsdal county, Norway: Examples for the hazard and potential of rock slide dams. In: Margottini, C., Canuti, P., Sassa, K. (eds): Landslide science and practice, 6: Risk Assessment, Management and Mitigation, Springer-Verlag, Berlin Heidelberg, Germany, 3-12, DOI 10.1007/978-3-642-31325-6_1, 2013.

Hermanns, R.L., Oppikofer, T., Roberts, N.J., and Sandøy, G.: Catalogue of historical displacement waves and landslide-triggered tsunamis in Norway, Engineering Geology for Society and Territory-Volume 4, Springer, 63-66, ISBN 3319086596, 2014.

Hermanns, R. L, Schleier, M., Bohme, M. Blikra, L. H., Gosse, J., Ivy-Ochs, S., Hilger, P.: Rock-avalanche activity in W and S Norway peaks after the retreat of the Scandinavian Ice Sheet. In: Mikoš M, Vilimek V, Yin Y et al. (eds) Advancing Culture of Living with Landslides. Cham: Springer, pp. 331–338, 2017.

Hipp, T., Etzelmüller, B., Farbrot, H. and Schuler, T. V.: Modelling the temperature evolution of permafrost and seasonal frost in southern Norway during the 20th and 21st century, The Cryosphere Discussions, 5(2), 811–854, doi:https://doi.org/10.5194/tcd-5-811-2011, 2011.

Hipp, T., Etzelmüller, B., Farbrot, H., Schuler, T. V. and Westermann, S.: Modelling borehole temperatures in Southern Norway – insights into permafrost dynamics during the 20th and 21st century, The Cryosphere, 6(3), 553–571, doi:https://doi.org/10.5194/tc-6-553-2012, 2012.

Hipp, T., Etzelmüller, B. and Westermann, S.: Permafrost in Alpine Rock Faces from Jotunheimen and Hurrungane, Southern Norway, Permafrost and Periglacial Processes, 25(1), 1–13, doi:10.1002/ppp.1799, 2014.

Hilger, P., Hermanns, R.. L., Gosse, J. C., Jacobs, B., Etzelmüller, B., Krautblatter, M.: Multiple rock-slope failures from Mannen in Romsdal Valley, western Norway, revealed from Quaternary geological mapping and 10Be exposure dating, The Holocene: 0959683618798165, 2018.

Huggel, C., Zgraggen-Oswald, S., Haeberli, W., Kääb, A., Polkvoj, A., Galushkin, I. and Evans, S. G.: The 2002 rock/ice avalanche at Kolka/Karmadon, Russian Caucasus: assessment of extraordinary avalanche formation and mobility, and application of QuickBird satellite imagery, Natural Hazards and Earth System Sciences, 5(2), 173–187, doi:https://doi.org/10.5194/nhess-5-173-2005, 2005.

Huggel, C., Allen, S., Deline, P., Fischer, L., Noetzli, J. and Ravanel, L.: Ice thawing, mountains falling—are alpine rock slope failures increasing?, Geology Today, 28(3), 98–104, doi:10.1111/j.1365-2451.2012.00836.x, 2012.

Hughes, A. L. C., Gyllencreutz, R., Lohne, Ø. S., Mangerud, J., Svendsen, J. I.: The last Eurasian ice sheets – a chronological database and time-slice reconstruction, Boreas, 45, 1-45, 10.1111/bor.12142, 2016

Isaksen, K., Hauck, C., Gudevang, E., Ødegård, R. S. and Sollid, J. L.: Mountain permafrost distribution in Dovrefjell and Jotunheimen, southern Norway, based on BTS and DC resistivity tomography data, Norsk Geografisk Tidsskrift - Norwegian Journal of Geography, 56(2), 122–136, doi:10.1080/002919502760056459, 2002.

Isaksen, K., Farbrot, H., Blikra, L. H. Johansen, B., and Sollid, J. L.: Five-year ground surface temperature measurements in Finnmark, northern Norway, Proceedings of the Ninth International Conference on Permafrost, edited by: Kane, D. L. and Hinkel, K. M., Institute of Northern Engineering, University of Alaska Fairbanks, Fairbanks, Alaska, USA, 789–794, 2008.

Isaksen, K., Ødegård, R. S., Etzelmüller, B., Hilbich, C., Hauck, C., Farbrot, H., Eiken, T., Hygen, H. O. and Hipp, T. F.: Degrading Mountain Permafrost in Southern Norway: Spatial and Temporal Variability of Mean Ground Temperatures, 1999–2009, Permafrost and Periglacial Processes, 22(4), 361–377, doi:10.1002/ppp.728, 2011.

IPCC, 2013. Climate Change 2013: The Physical Science Basis. Contribution of Working Group I to the Fifth Assessment Report of the Intergovernmental Panel on Climate Change. Cambridge University Press, Cambridge, United Kingdom and New York, NY, USA, 1535 pp.

Juliussen, H. and Humlum, O.: Thermal regime of openwork block fields on the mountains Elgåhogna and Sølen, central-eastern Norway, Permafrost and Periglacial Processes, 19(1), 1–18, doi:10.1002/ppp.607, 2008.

King, L. High mountain permafrost in Scandinavia, 4th International Conference on Permafrost, Proceedings, National Academy Press, Washington, DC, 612-617, 1983.

5   King, L.: Zonation and ecology of high mountain permafrost in Scandinavia, Geografiska Annaler Series A: Physical Geography, 68, 131-139, 1986.

Kleman, J., and Hättestrand, C.: Frozen-bed Fennoscandian and Laurentide ice sheets during the Last Glacial Maximum: Nature, 402, 63-66, 1999.

Kleman, J., Stroeven, A.P., Lundqvist, J.: Patterns of Quaternary ice sheet erosion and deposition in
10   Fennoscandia and a theoretical framework for explanation, Geomorphology, 97 (1–2), 73–90, 2008.

Korup, O.: Linking landslides, hillslope erosion, and landscape evolution, Earth Surface Processes and Landforms, 34(9), 1315–1317, doi:10.1002/esp.1830, 2009.

Krautblatter, M., Funk, D. and Günzel, F. K.: Why permafrost rocks become unstable: a rock–ice- mechanical model in time and space - Krautblatter - 2013 - Earth Surface Processes and Landforms - Wiley Online Library,
15   [online] Available from: https://onlinelibrary.wiley.com/doi/full/10.1002/esp.3374 (Accessed 12 November 2018), 2013.

Lilleøren, K. S., Etzelmüller, B.: A regional inventory of rock glaciers and ice-cored moraines in Norway. Geografiska Annaler. Series A, Physical Geography 93: 175–191. DOI:10.1111/j.1468-0459.2011.00430.x, 2011.

20   Lussana, C., Tveito, O. E. and Uboldi, F.: Three-dimensional spatial interpolation of 2 m temperature over Norway, Quarterly Journal of the Royal Meteorological Society, 144(711), 344–364, doi:10.1002/qj.3208, 2017.

Magnin, F., Deline, P., Ravanel, L., Noetzli, J. and Pogliotti, P.: Thermal characteristics of permafrost in the steep alpine rock walls of the Aiguille du Midi (Mont Blanc Massif, 3842 m a.s.l), The Cryosphere, 9(1), 109–121, doi:https://doi.org/10.5194/tc-9-109-2015, 2015a.

25   Magnin, F., Brenning, A., Bodin, X., Deline, P. and Ravanel, L.: Modélisation statistique de la distribution du permafrost de paroi : application au massif du Mont Blanc, Géomorphologie : relief, processus, environnement, 21(vol. 21 – n° 2), 145–162, doi:10.4000/geomorphologie.10965, 2015b.

Magnin, F., Josnin, J.-Y., Ravanel, L., Pergaud, J., Pohl, B. and Deline, P.: Modelling rock wall permafrost degradation in the Mont Blanc massif from the LIA to the end of the 21st century, The Cryosphere, 11(4), 1813–
30   1834, doi:https://doi.org/10.5194/tc-11-1813-2017, 2017a.

Magnin, F., Westermann, S., Pogliotti, P., Ravanel, L., Deline, P. and Malet, E.: Snow control on active layer thickness in steep alpine rock walls (Aiguille du Midi, 3842 m a.s.l., Mont Blanc massif)., CATENA, 149, p648–p662, 2017b.

Matsuoka, N. and Murton, J.: Frost weathering: recent advances and future directions, Permafrost and Periglacial
35   Processes, 19(2), 195–210, doi:10.1002/ppp.620, 2008.

Myhra, K. S., Westermann, S. and Etzelmüller, B.: Modelled Distribution and Temporal Evolution of Permafrost in Steep Rock Walls Along a Latitudinal Transect in Norway by CryoGrid 2D, Permafrost and Periglacial Processes, 28(1), 172–182, doi:10.1002/ppp.1884, 2017.

Noetzli, J. and Gruber, S.: Transient thermal effects in Alpine permafrost, The Cryosphere, 3(1), 85–99,
40   doi:10.5194/tc-3-85-2009, 2009.

Ødegård, R. S., Sollid, J. L. and Liestøl, O.: Ground temperature measurements in mountain permafrost, Jotunheimen, southern Norway, Permafrost and Periglacial Processes, 3(3), 231–234, doi:10.1002/ppp.3430030310, 1992.

Oppikofer, T., Nordahl, B., Bunkholt, H., Nicolaisen, M., Jarna, A., Iversen, S., Hermanns, R. L., Böhme, M.
45   and Yugsi Molina, F. X.: Database and online map service on unstable rock slopes in Norway — From data perpetuation to public information, Geomorphology, 249, 69–81, doi:10.1016/j.geomorph.2015.08.005, 2015.

Ravanel, L., Magnin, F. and Deline, P.: Impacts of the 2003 and 2015 summer heatwaves on permafrost-affected rock-walls in the Mont Blanc massif, Science of The Total Environment, 609, 132–143, doi:10.1016/j.scitotenv.2017.07.055, 2017.

Romstad, B., Harbitz, C. B. and Domaas, U.: A GIS method for assessment of rock slide tsunami hazard in Norwegian lakes and reservoirs, Natural hazards and earth system sciences, 9(2), 353–364, doi:http://dx.doi.org/10.5194/nhess-9-353-2009, 2009.

Sellier, D.: Le felsenmeer du Mont Gausta (Telemark, Norvège) : environnement, caractères morphologiques et significations paléogéographiques, Géographie physique et Quaternaire, 49(2), 185–205. doi:10.7202/033036ar, 1995.

Sollid, J. L., & Sørbel, L. Palsa bogs as a climate indicator: examples from Dovrefjell, southern Norway. Ambio, 287-291, 1998.

Sollid, J., Isaksen, K., Eiken, T., and Ødegård, R.: The transition zone of mountain permafrost on Dovrefjell, southern Norway, in: Proceedings of the International Conference on Permafrost, 2, 1085–1090, 2003.

Sosio, R., Crosta, G. B. and Hungr, O.: Complete dynamic modeling calibration for the Thurwieser rock avalanche (Italian Central Alps), Engineering Geology, 100(1), 11–26, doi:10.1016/j.enggeo.2008.02.012, 2008.

Steiger, C., Etzelmüller, B., Westermann, S. and Myhra, K. S.: Modelling the permafrost distribution in steep rock walls, Norwegian Journal of Geology, doi:10.17850/njg96-4-04, 2016.

Westermann, S., Schuler, T. V., Gisnås, K. and Etzelmüller, B.: Transient thermal modeling of permafrost conditions in Southern Norway, The Cryosphere, 7(2), 719–739, doi:10.5194/tc-7-719-2013, 2013.
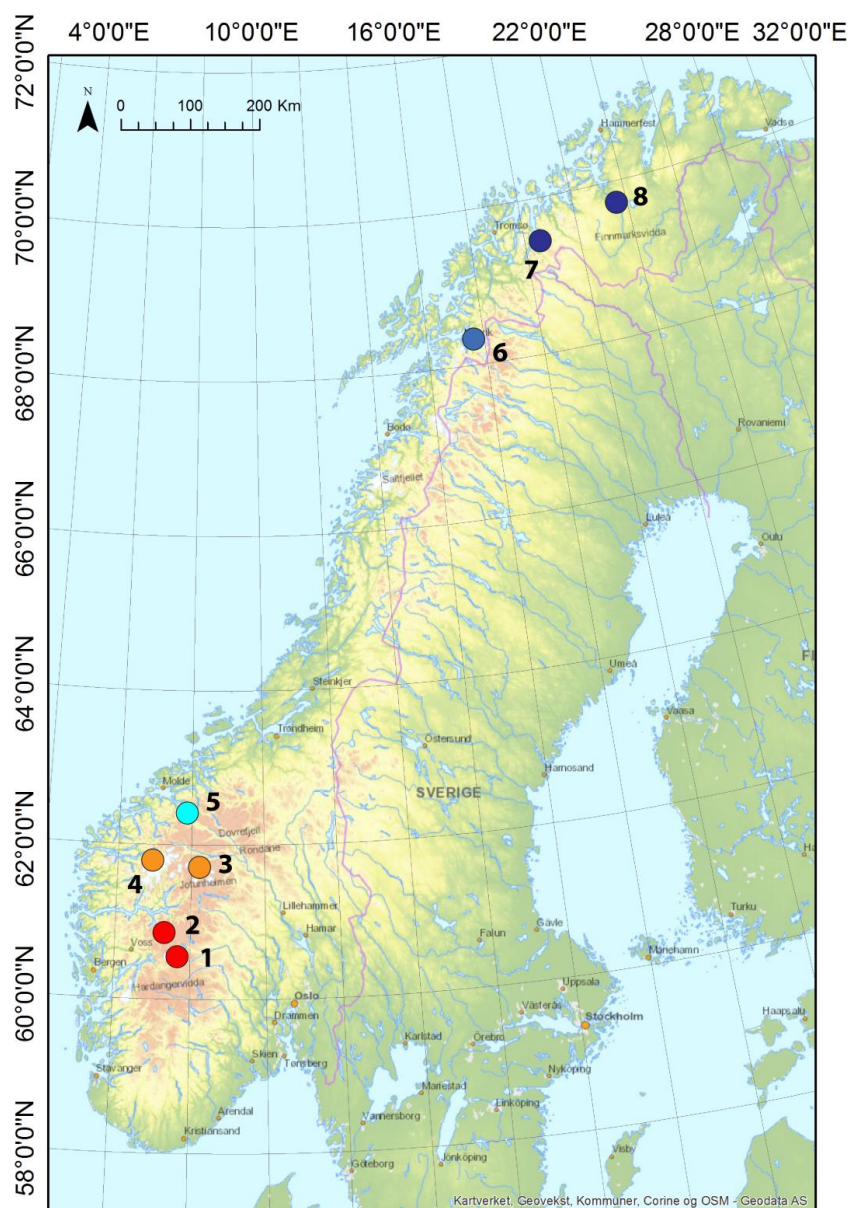
Figure

Figure 1. Location of the rock surface temperature loggers in steep slopes across Norway. **1.** Finse (1 logger). **2.** Flåm (3 loggers). **3.** Jotunheimen (4 loggers). **4.** Loen (3 loggers). **5.** Mannen (2 loggers). **6.** Narvik (3 loggers). **7.** Kåfjord (7 loggers). **8.** Alta (2 loggers). The color range is adapted to latitude in accordance with Figure 2.
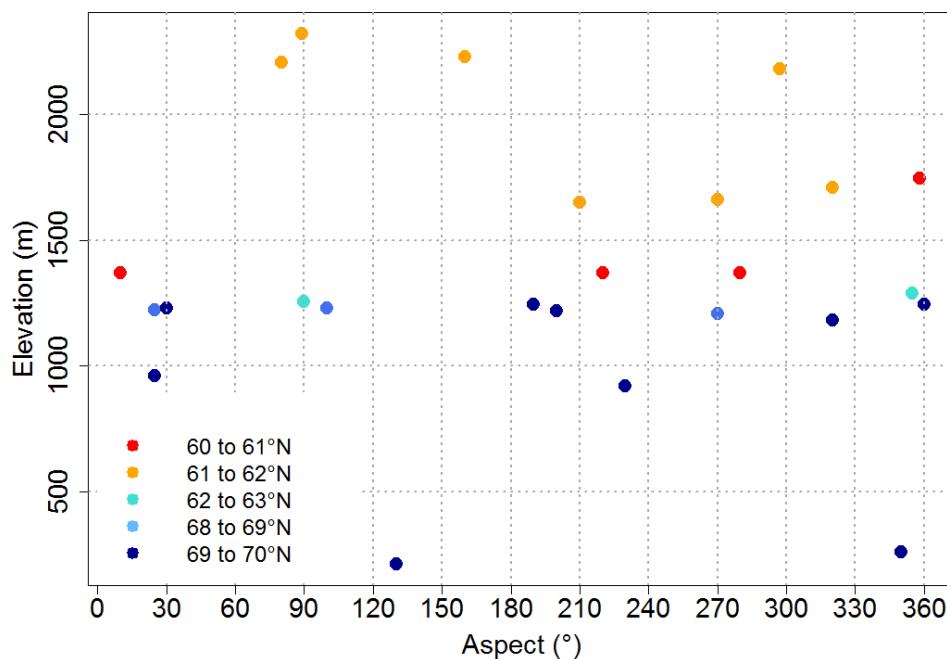
Figure 2. Distribution of the 25 loggers according to elevation, aspect and latitude.
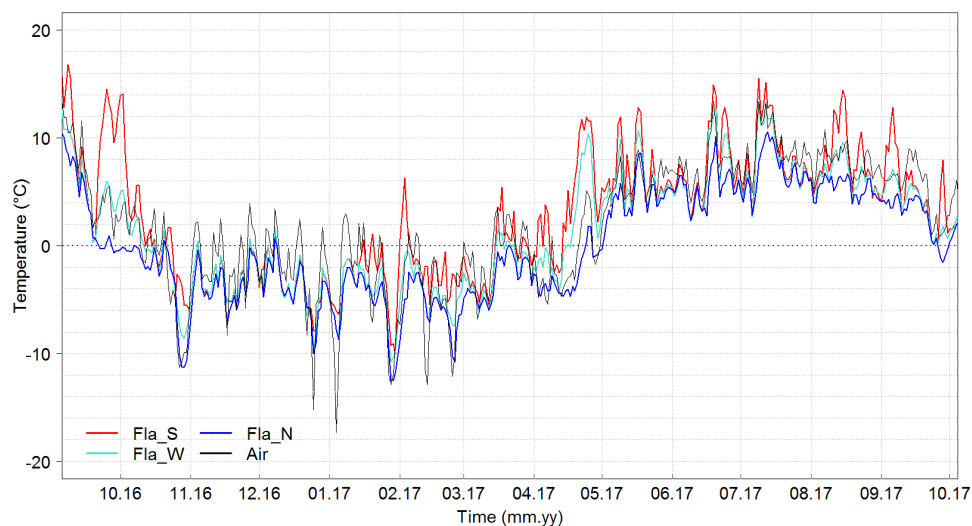
Figure 3. Example of daily rock surface temperature data for the site of Flåm during one hydrological year.
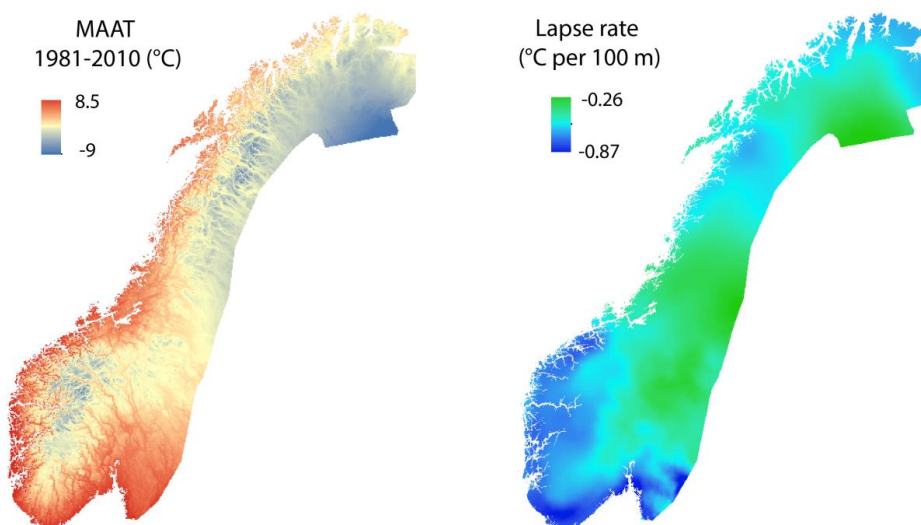
Figure 4. 1km grid Mean Annual Air Temperature (MAAT) derived from the SeNorge2 dataset (left, Lussana et al., 2017) and averaged lapse rate over a 25 km radius (right).
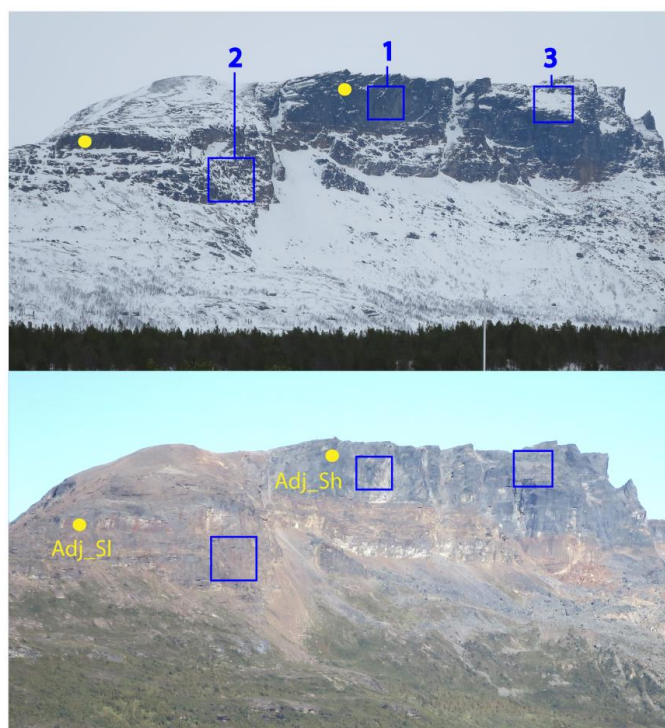
Figure 5. Pictures of the Ádjit crest (top: March 2017, bottom: August 2018 showing variable bedrock settings more or less favorable to permafrost occurrence. 1. Vertical and compact bedrock. 2. Fractured bedrock and sparse snow deposits. 3. Highly fractured slope with substantial snow and debris accumulations.
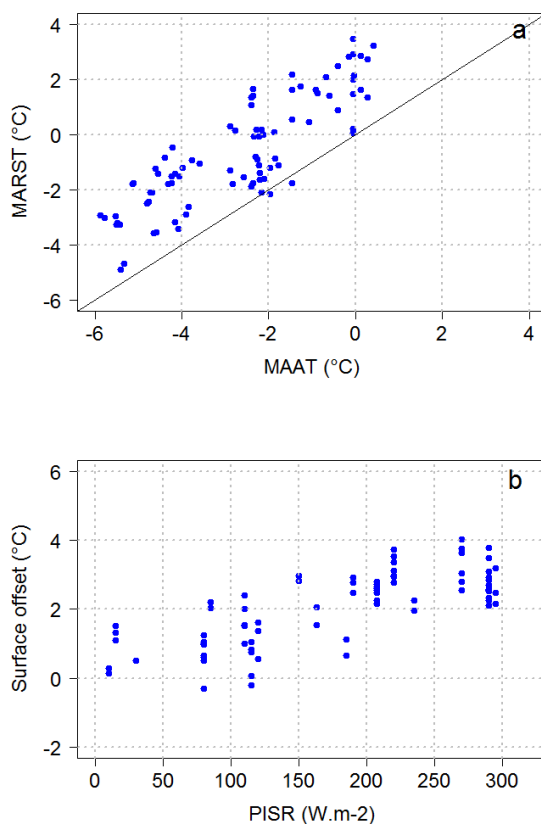
Figure 6. a. Measured Mean Annual Rock Surface Temperature (MARST) *versus* interpolated MAAT at the MARST measurement points. **b.** Surface offset (*i.e.* MARST measured – MAAT interpolated) *versus* calculated Potential Incoming Solar Radiation (PISR) at measurement points. The multiple MARST points for a same PISR values result of the multiple years of RST records at a same logger, and for which the PISR value remains identical.
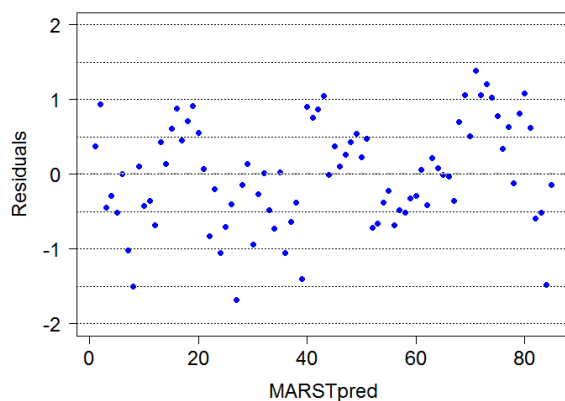
Figure 7. Residuals of the predicted MARST.
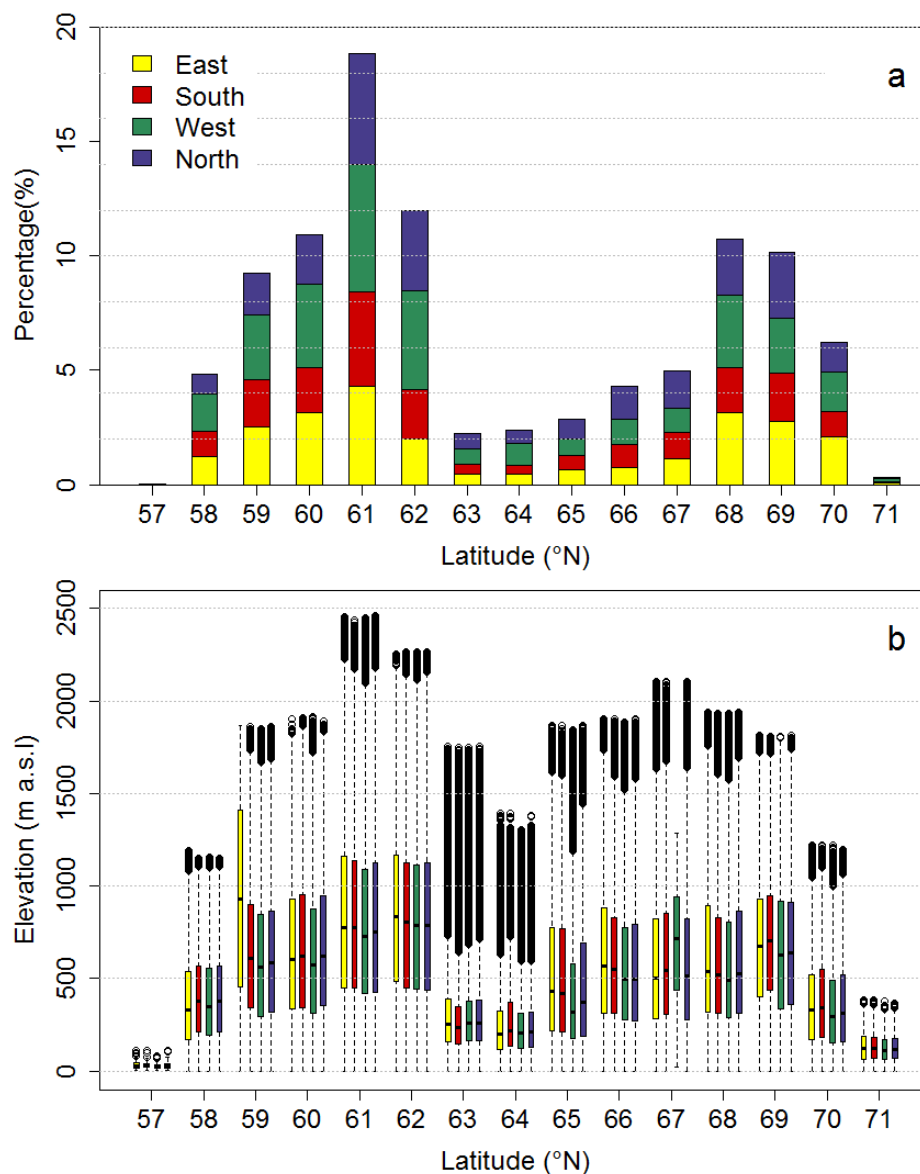
Figure 8. Relative distribution of steep rock walls across Norway (slopes > 40° based on the 10 m resolution DEM). **a.** Relative distribution of rock wall surface area according to aspect and latitude. **b.** Relative distribution of rock wall according to latitude and aspect and elevation. East: 45 to 135°; South: 135 to 225°; West: 225 to 315°; North: 315 to 45°.

The lowest and highest boundaries of the boxes respectively display the 1st and 3rd quartile (Q1 and Q3) of the observations. The lowest and highest whiskers respectively show Q1-((Q3-Q1)×1.5]) and (Q3+((Q3-Q1)×1.5)). The dots are the outliers.
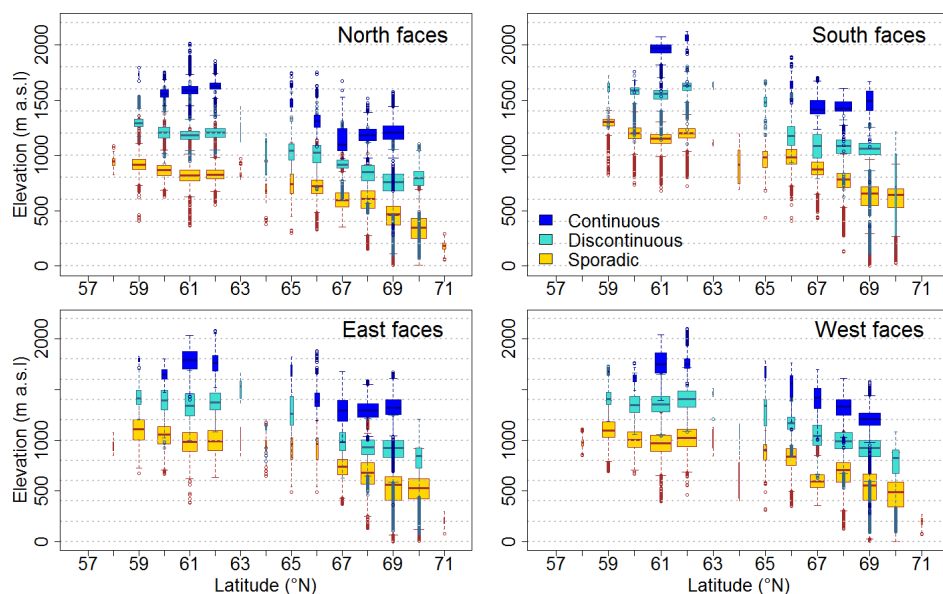
Figure 9. Distribution of the lower limit of each permafrost class according to elevation, aspect and latitude. The width of the boxes is proportional to the square-roots of the number of observations in the respective groups. The lowest and highest boundaries of the boxes respectively display the 1st and 3rd quartile (Q1 and Q3) of the observations. The lowest and highest whiskers respectively show Q1-((Q3-Q1)×1.5]) and (Q3+((Q3-Q1)×1.5)). The dots are the outliers.
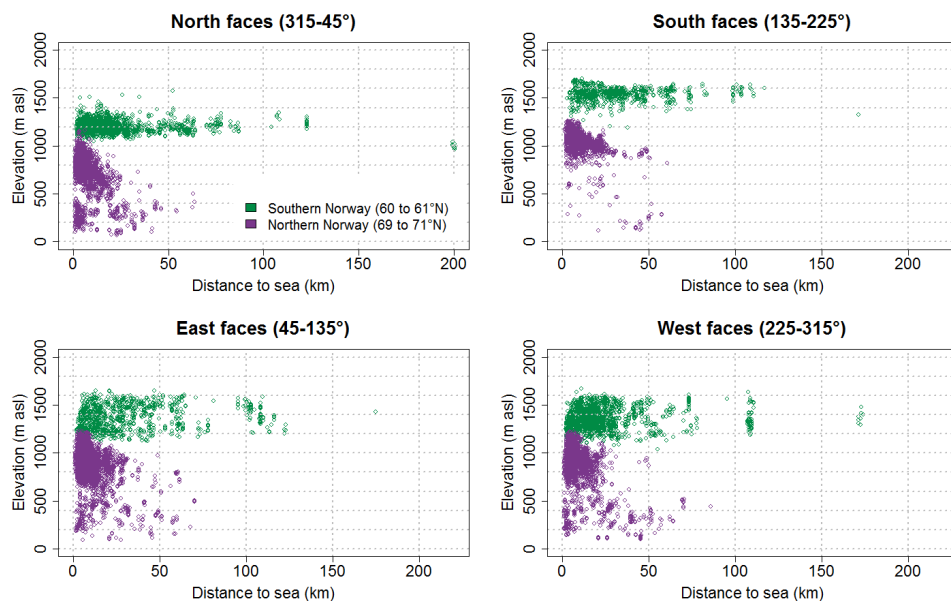
Figure 10. Distribution of the lower limit of discontinuous permafrost in Southern and Northern Norway according the distance to the sea.
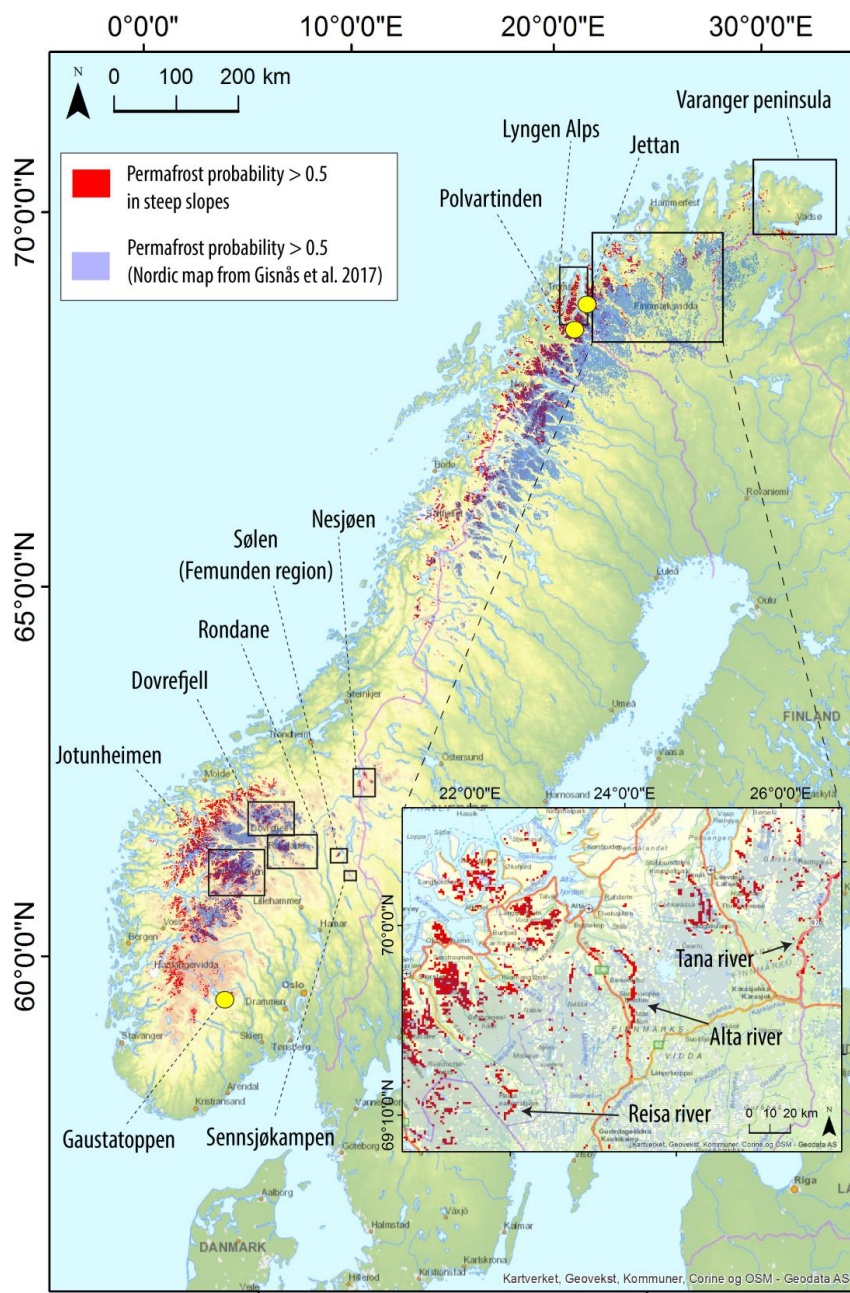
Figure 11. Permafrost distribution in steep slopes of Norway according to the CryoWall map and in Scandinavia according to the map produced by Gisnåas et al. (2017). Areas of interest for the discussion are displayed.
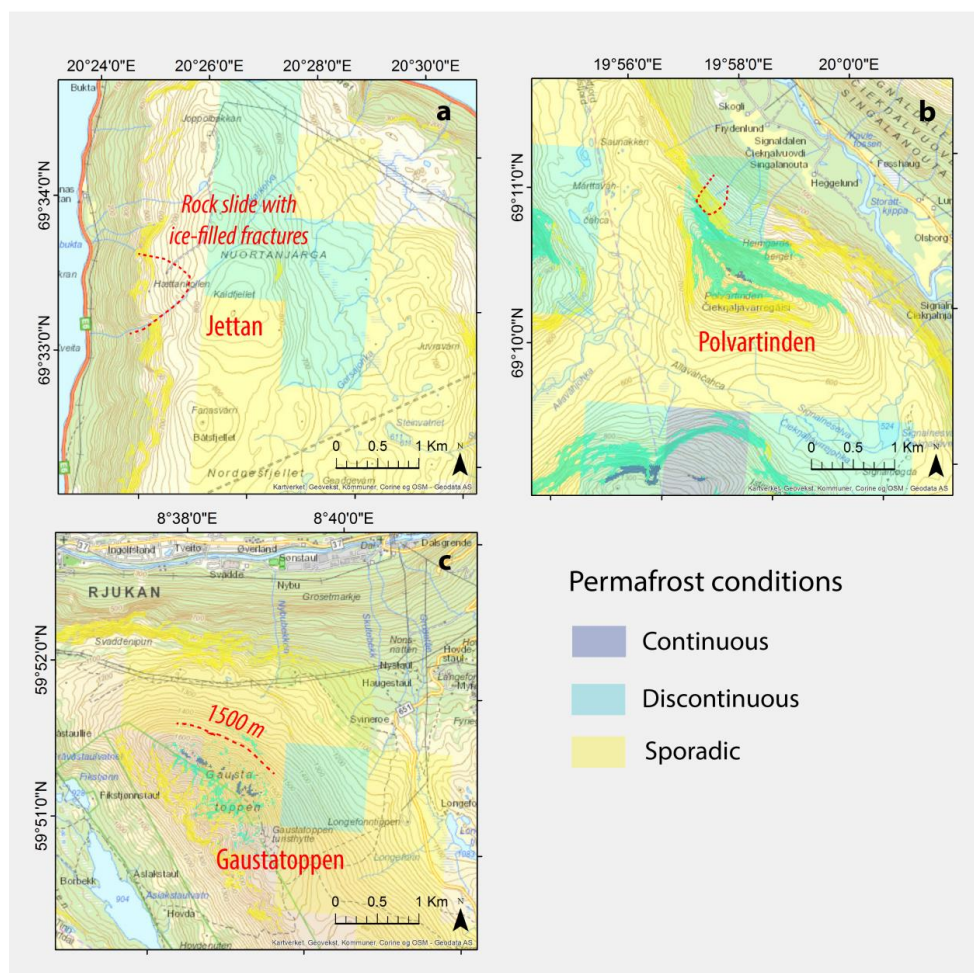
Figure 12. Permafrost distribution at steep slope sites where permafrost has been previously observed in Norway (a. Blikra and Christiansen, 2014; b. Frauenfelder et al., 2018; Etzelmuller et al., 2003b). The CryoWall map has been combined with the 1 km resolution Nordic permafrost map (Gisnås et al., 2017) to display predicted permafrost in all types of terrains.
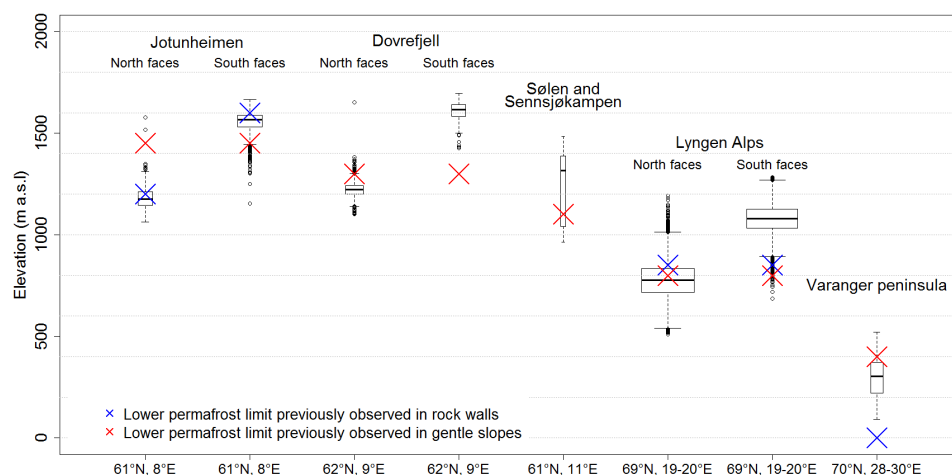
Figure 13. Comparison of steep slopes permafrost distribution in specific regions with estimations from previous studies (Hipp et al., 2014; Isaksen et al., 2002; 2008; 2011; Farbrot et al., 2011; 2013; Sollid et al., 2003; Westermann et al., 2013; Heggem et al., 2005; Steiger et al., 2016; Gisnås et al., 2017; Borge et al., 2017). The width of the boxes is proportional to the square-roots of the number of observations in the respective groups.

Tables

Area	ID	Latitude, Longitude	Elevation (m asl)	Aspect (°)	Date of installation
(1) Finse	Fin_N	60°33'25.6"N, 7°27'40.2"E	1743	358	23.09.2017
(2) Flåm	Fla_S	60° 50' 35.9"N, 7° 9' 52.7"E	1370	220	11.08.2016
	Fla_N	60° 50' 41.1"N, 7° 9' 47.2"E	1370	10	11.08.2016
	Fla_W	60° 50' 40.6"N, 7° 9' 46.8"E	1370	280	11.08.2016
(3) Jotun-heimen	Juv_El	61°39'12.4" 8°19'36.6"E	2204	82	26.09.2010
	Juv_S	61° 39' 0.7" N 8° 18' 43.9"E	2226	162	26.09.2010
	Juv_W	61° 38' 48.4" N 8° 18' 32.1"E	2179	297	27.09.2010
	Juv_Eh	61° 38' 27.4" N 8° 18' 22.4"E	2320	89	27.09.2010
(4) Loen	Loe_S	61° 49' 32.0" N 7° 1' 20.5"E	1648	210	13.08.2015
	Loe_W	61° 49' 32.4" N 7° 1' 27.3"E	1662	270	13.08.2015
	Loe_N	61° 49' 17.3"N, 7° 1' 48.7"E	1709	320	13.08.2015
(5) Mannen	Man_E	62° 27' 21.5"N, 7° 46' 45.0"E	1290	90	06.08.2015
	Man_N	62° 27' 21.4"N, 7° 46' 45.2"E	1290	350	06.08.2015
(6) Narvik	Nar_N	68° 26' 1.8" N, 17° 34' 49.9"E	1224	25	29.08.2016
	Nar_E	68° 26' 1.5" N, 17° 34' 50.3"E	1228	100	29.08.2016
	Nar_W	68° 26' 3.0" N, 17° 34' 40.9"E	1208	270	29.08.2016
(7) Kåfjord	Anka_N	69° 28' 34.7" N, 20° 29' 30.2"E	960	25	25.08.2015
	Gam_S	69° 28' 53.5" N, 20° 34' 28.1"E	1220	200	25.08.2015
	Gam_W	69° 28' 53.6" N, 20° 34' 28.2"E	1183	320	25.08.2015
	Gam_N	69° 28' 59.3" N, 20° 34' 42.0"E	1243	360	25.08.2015
	Adj_Sl	69° 22' 25.2" N, 20° 23' 25.3"E	920	230	24.08.2015
	Adj_Sh	69° 22' 3.5" N, 20° 25' 20.4"E	1245	190	24.08.2015
	Adj_N	69° 22' 3.2" N, 20° 25' 24.1"E	1230	30	24.08.2015
(8) Alta	Alt_N	69 46' 04.3''N, 23 41'47.0''E	260	350	03.09.2016
	Alt_S	69 46'12.6''N, 23 41'33.7''E	215	130	03.09.2016

Table 1. Settings of the temperature sensors used in this study

ID	Aver. Period*	Nb of days missing for **	Weather station name and elevation (m asl.) ***	Correlation with RST****
Fin_Nl	NoData	0	-	-
Fin_Nh	25.09. to 24.09	0	-	-
Fla_S	15.08 to 14.08	0	-	-
Fla_N	15.08 to 14.08	0	-	-
Fla_W	15.08 to 14.08	0	-	-
Juv_El	28.09 to 27.09	21	Sogneflehytta (1413)	0.8264
Juv_S	28.09 to 27.09	21	Juvasshøe (1894)	0.8153
Juv_W	28.09 to 27.09	21	Sogneflehytta (1413)	0.8384
Juv_Eh	28.09 to 27.09	21	Juvasshøe (1894)	0.7741
Loe_S	15.08 to 14.08	0	-	-
Loe_W	15.08 to 14.08	0	-	-
Loe_N	15.08 to 14.08	0	-	-
Man_E	07.08 to 06.08	6	Mannen (1294)	0.87
Man_N	07.08 to 06.08	6	Mannen (1294)	0.91
Rom_N	30.08 to 29.08	0	-	-
Rom_E	30.08 to 29.08	0	-	-
Rom_W	30.08 to 29.08	0	-	-
Anka_N	01.09 to 31.08	0	-	-
Gam_S	01.09 to 31.08	0	-	-
Gam_W	01.09 to 31.08	0	-	-
Gam_N	01.09 to 31.08	0	-	-
Adj_Sl	01.09 to 31.08	0	-	-
Adj_Sh	01.09 to 31.08	0	-	-
Adj_N	01.09 to 31.08	0	-	-
Alt_N	04.09 to 03.09	4	Alta airport (3)	0.942
Alt_S	04.09 to 03.09	4	Alta airport (3)	0.9109

Averaging period for the MARST calculation

** *Number of days missing for the calculation of the most recent MARST*

*** *Elevation of the weather station chosen to reconstruct the daily RST during the missing days*

**** *Correlation between the daily RST and the daily AT recorded at the weather station*

Table 2. Summary of the data used for calculating the MARST

ID	Weather stations name, date of installation and elevations (m asl.)	Correlation with RST	Missing data during the period (%)
Fin_Nh	960 Midstova, November 2011, 1162	0.9398 0.9499	0
Fla_S		0.7693 0.7438	
Fla_N	Klevavatnet, November 2013 (960) Vestredalen, January 2012 (1160)	0.9297 0.9358	0 18.2
Fla_W		0.8897 0.874	
Juv_El		0.8264 0.8103	
Juv_S	Sognefjellhytta, December 1978 (1413) Juvasshytta, September 1999 (1894)	0.805 0.8153	
Juv_W		0.8384 0.812	0 0
Juv_Eh		0.7741 0.7444	
Loe_S		0.7504 0.7119	
Loe_W	Utvikfjellet, August 2011 (635) Trolledalsegga, October 2015 (1020)	0.7997 0.7676	21.6 4.8
Loe_N		0.9422 0.915	
Man_E	Marstein, February 2010 (67) Mannen, March 2010 (1294)	0.8139 08768	
Man_N		0.8625 0.9065	0.5 2.6
Rom_N		0.8912 0.8835	
Rom_E	Straumsnes, January 2011 (200) Fagernesfjellet, January 1979 (1000)	0.8628 0.8606	0 0
Rom_W		0.8836 0.8884	
Anka_N		0.872 0.8383	
Gam_S		0.8407 0.7719	
Gam_W		0.8828 0.874	
Gam_N	Skibotn II (20) Jettan, July 2015 (691)	0.8452 0.8458	3.3 0
Adj_Sl		0.8795 0.8521	
Adj_Sh		0.8459 0.7712	
Adj_N		0.8898 0.8556	
Alt_N	Alta airport, December 1963 (3) Sihccajavri, April 2013 (382)	0.942 0.9241	0
Alt_S		0.9109 0.9003	0

Table 3. Summary of the data used for the MAAT calculation

	Min	Mean	Median	Max
MARST (°C)	-4.9	-0.6	-1.05	3.5
MAAT (°C)	-5.9	-2.6	-2.4	0.4
PISR (W m^{-2})	10	179	208	295

Table 4. Summary of the model variables

Intercept	0.478*
PISR (Wm^{-2})	0.0097***
MAAT (°C)	1.06***
R^2	0.88
R$^2_{adj}$	0.88
R$^2_{cv}$	0.88
RMSE (°C)	0.63
RMSE$_{cv}$ (°C)	0.69
MAE (°C)	0.56
MAE$_{cv}$ (°C)	0.58
Standard deviation (°C)	1.86
Residual standard error (°C)	0.699
p-value	< 2.2e-16

Table 5. Summary statistics of the model. Significance of Wald test: *<0.05, ***<0.001